

1 Quasi-consistent efficient meshfree thin shell
2 formulation to naturally accommodate essential
3 boundary conditions

4 Junchao Wu^{a,*}, Yangtao Xu^b, Bin Xu^a, Syed Humayun Basha^{c,*}

^a*Key Laboratory for Intelligent Infrastructure and Monitoring of Fujian Province, College
of Civil Engineering, Huaqiao University, Xiamen, Fujian, 361021, China*

^b*College of Civil Engineering, Huaqiao University, Xiamen, Fujian, 361021, China*

^c*Key Laboratory for Structural Engineering and Disaster Prevention of Fujian Province,
College of Civil Engineering, Huaqiao University, Xiamen, Fujian, 361021, China*

5 **Abstract**

This research proposed an efficient and quasi-consistent meshfree thin shell formulation with natural enforcement of essential boundary conditions. Within the framework of the Hu-Washizu variational principle, a mixed formulation of displacements, strains and stresses is employed in this approach, where the displacements are discretized using meshfree shape functions, and the strains and stresses are expressed using smoothed gradients, covariant smoothed gradients and covariant bases. The smoothed gradients satisfy the first and second order integration constraint and have quasi-consistent consistency. Owing to Hu-Washizu variational principle, the essential boundary conditions automatically arise in its weak form. As a result, the suggested technique's enforcement of essential boundary conditions resembles that of the traditional Nitsche's method. Contrary to Nitsche's method, the costly higher order derivatives of conventional meshfree shape functions were replaced by the smoothed gradients with fast computation, which improve the efficiency. Meanwhile, the proposed formulation features a naturally stabilized term without adding any artificial stabilization factors, which eliminates the stabilization parameter-dependent issue in the Nitsche's method. The efficacy of the proposed Hu-Washizu meshfree thin shell formulation is illustrated by a set of classical standard thin shell problems.

6 *Keywords:* Meshfree, Thin shell, Hu-Washizu variational principle,
7 Reproducing kernel gradient smoothing, Essential boundary condition

*Corresponding author

Email addresses: jcwu@hqu.edu.cn (Junchao Wu), syedhbasha@hqu.edu.cn (Syed Humayun Basha)

8 1. Introduction

9 Thin shell structures generally adhere to the Kirchhoff hypothesis [1], that
10 neglects the shear deformation can be described using Galerkin formulation
11 which requires to have at least C^1 continuity. The traditional finite element
12 methods usually only have C^0 continuous shape functions, and it prefers Mindlin
13 thick shear theory, hybrid and mixed models in simulation of shell structure [2].
14 Meshfree methods [3, 4, 5] with high order smoothed shape functions have gar-
15 nered much research attention over the past thirty years. These techniques
16 established the shape functions based on a collection of dispersed nodes, and
17 the high order continuity of shape functions can be easily achieved even with
18 low-order basis functions. For thin shell analysis, this high order meshfree ap-
19 proximation can also alleviate the membrane locking caused by the mismatched
20 approximation order of membrane strain and bending strain [6]. Furthermore,
21 nodal-based meshfree approximations generally offer the flexibility of local re-
22 finement and can relieve the burden of mesh distortion. Owing to these benefits,
23 numerous meshfree techniques have been developed and implemented in many
24 scientific and engineering fields [7, 8, 9, 10, 11, 12]. However, the high order
25 smoothed meshfree shape functions accompany the enlarged and overlapping
26 supports, which may potentially cause many problems for shape functions. One
27 of the issues is the loss of the Kronecker delta property, which means that, un-
28 like the finite element methods, the necessary boundary conditions cannot be
29 directly enforced [13]. Another issue is that the variational consistency or said
30 integration constraint cannot be satisfied due to the misalignment between the
31 numerical integration domains and supports of shape functions. Besides, the
32 shape functions exhibit a piecewise rational nature in each integration domain.
33 Therefore, variational consistency is vital to the solution accuracy in Galerkin
34 formulations [14, 15].

35 Various ways have been presented to enforce the necessary boundary for
36 Galerkin meshfree methods directly, including the boundary singular kernel
37 method [16], mixed transformation method [16], and interpolation element-free
38 method [17] for recovering shape functions' Kronecker property. However, these
39 methods are not based on a variational setting and cannot guarantee variational
40 consistency. In the absence of a meshfree node, accuracy enforcement might be
41 poorer. In contrast, enforcing the essential boundary conditions using a vari-
42 ational approach is preferred for Galerkin meshfree methods. The variational
43 consistent Lagrange multiplier approach was initially used to the Galerkin mesh-
44 free method by Belytschko et al. [3]. In this method, the extra degrees of free-
45 dom are used to determine the discretion of Lagrange multiplier. Furthermore,
46 Ivannikov et al. [18] have extended this approach to geometrically nonlinear
47 thin shells. Lu et al. [19] suggested the modified variational essential bound-
48 ary enforcement approach and expressed the Lagrange multiplier by equivalent
49 tractions to eliminate the excess degrees of freedom. However, the coercivity
50 of this approach is not always ensured and potentially reduces the accuracy.
51 Zhu and Atluri [20] pioneered the penalty method for meshfree method, mak-
52 ing it a straightforward approach to enforce essential boundary conditions via

53 Galerkin weak form. However, the penalty method lacks variational consistency
54 and requires experimental artificial parameters whose optimal value is hard to
55 determine. Fernández-Méndez and Huerta [13] imposed necessary boundary
56 conditions using Nitsche’s approach in the meshfree formulation. This approach
57 can be seen as a hybrid combination of the modified variational method and the
58 penalty method because the modified variational method generates variational
59 consistency through the use of a consistent term, and the penalty method is
60 used as a stabilized term to recover the coercivity. Skatulla and Sansour [21]
61 extended Nitsche’s thin shell analysis method and proposed an iteration algo-
62 rithm to determine artificial parameters at each integration point.

63 In order to address the issue of numerical integration, a series of consis-
64 tent integration schemes have been developed for Galerkin meshfree methods.
65 Among these include stabilized conforming nodal integration [22], variational
66 consistent integration [23], quadratic consistent integration [24], reproducing
67 kernel gradient smoothing integration [25], and consistent projection integration
68 [26]. The assumed strain approach establishes the most consistent integration
69 scheme, while the smoothed gradient replaces the costly higher order derivatives
70 of traditional meshfree shape functions and shows a high efficiency. Moreover,
71 to achieve global variational consistency, a consistent essential boundary con-
72 dition enforcement should cooperate with the consistent integration scheme.
73 The consistent integration scheme and Nitsche’s method for treating essential
74 boundary conditions show a good performance since they can satisfy the coer-
75 civity without requiring additional degrees of freedom. Nevertheless, Nitsche’s
76 approach still retains the artificial parameters in stabilized terms, and it is es-
77 sential to remain conscious of the costly higher order derivatives, particularly
78 for thin plate and thin shell problems. Recently, Wu et al. [27, 28] proposed
79 an efficient and stabilized essential boundary condition enforcement method
80 based upon the Hellinger-Reissner variational principle, where a mixed formu-
81 lation in Hellinger-Reissner weak form recasts the reproducing kernel gradient
82 smoothing integration. The terms for enforcing essential boundary conditions
83 are identical to the Nitsche’s method, and both have consistent and stabilized
84 terms. Nevertheless, the stabilized term of this method naturally exists in the
85 Hellinger-Reissner weak form and no longer needs the artificial parameters, even
86 for essential boundary enforcement; instead all of the higher order derivatives
87 are represented by smoothed gradients and their derivatives.

88 In this study, an efficient and stabilized variational consistent meshfree
89 method that naturally enforces the essential boundary conditions is developed
90 for thin shell structure. Following the concept of the Hellinger-Reissner prin-
91 ciple base consistent meshfree method, the Hu-Washizu variational principle of
92 complementary energy with variables of displacement, strains, and stresses is
93 employed. The displacement is approximated by conventional meshfree shape
94 functions, and the strains and stresses are expressed by smoothed gradients with
95 covariant bases. It is important to note that although the first second-order in-
96 tegration requirements are naturally embedded in the smoothed gradients, their
97 fulfillment can only result in a quasi-satisfaction of variational consistency be-
98 cause of the non-polynomial nature of the stresses. Hu-Washizu’s weak form is

99 used to evaluate all the essential boundary conditions regarding displacements
100 and rotations. This type of formulation is similar to the Nitsche's method but
101 does not require any artificial parameters. Compared with Nitsche's method,
102 conventional reproducing smoothed gradients and its direct derivatives replace
103 the costly higher order derivatives. By utilizing the advantages of a replicating
104 kernel gradient smoothing framework, the smoothed gradients showed better
105 performance compared to conventional derivatives of shape functions, hence
106 increasing the meshfree formulation's computational efficiency.

107 The remainder of this research paper is structured as follows: The kinematics
108 of the thin shell structure and the weak form of the associated Hu-Washizu
109 principle are briefly described in Section 2. Subsequently, the mixed formulation
110 regarding the displacements, strains and stresses in accordance with Hu-Washizu
111 weak form are presented in Section 3. The discrete equilibrium equations are
112 derived in Section 4 using the naturally occurring accommodation of essential,
113 and they are compared to the equations obtained using Nitsche's method. The
114 numerical results in Section 5 validate the efficacy of the proposed Hu-Washizu
115 meshfree thin shell formulation. Lastly, the concluding remarks are presented
116 in Section 6.

117 2. Hu-Washizu's formulation of complementary energy for thin shell

118 2.1. Kinematics for thin shell

119 Consider the configuration of a shell $\bar{\Omega}$, as shown in Fig. 1, which can be
 120 easily described by a parametric curvilinear coordinate system $\boldsymbol{\xi} = \{\xi^i\}_{i=1,2,3}$.
 121 The mid-surface of the shell denoted by Ω is specified by the in-plane coordinates
 122 $\boldsymbol{\xi} = \{\xi^\alpha\}_{\alpha=1,2}$, as the thickness direction of shell is by ξ^3 , $-\frac{h}{2} \leq \xi^3 \leq \frac{h}{2}$, h is
 123 the thickness of shell. In this work, Latin indices take the values from 1 to 3,
 124 and Greek indices are evaluated by 1 or 2. For the Kirchhoff hypothesis [6], the
 125 position $\mathbf{x} \in \bar{\Omega}$ is defined by linear functions with respect to ξ^3 :

$$\mathbf{x}(\xi^1, \xi^2, \xi^3) = \mathbf{r}(\xi^1, \xi^2) + \xi^3 \mathbf{a}_3(\xi^1, \xi^2) \quad (1)$$

in which \mathbf{r} means the position on the mid-surface of shell, and \mathbf{a}_3 is correspond-

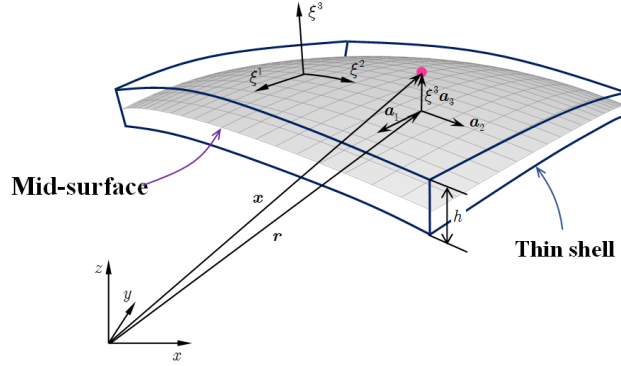


Figure 1: Kinematics for thin shell.

126 ing normal direction. For the mid-surface of shell, the in-plane covariant base
 127 vector with respect to ξ^α can be derived by a trivial partial differentiation to \mathbf{r} :
 128

$$\mathbf{a}_\alpha = \frac{\partial \mathbf{r}}{\partial \xi^\alpha} = \mathbf{r}_{,\alpha}, \alpha = 1, 2 \quad (2)$$

129 to provide for a clear expression, the subscript comma denotes the partial dif-
 130 ferentiation operation with respect to in-plane coordinates ξ^α , and the normal
 131 vector \mathbf{a}_3 can be obtained by the normalized cross product of \mathbf{a}_α 's as follows:

$$\mathbf{a}_3 = \frac{\mathbf{a}_1 \times \mathbf{a}_2}{\|\mathbf{a}_1 \times \mathbf{a}_2\|} \quad (3)$$

132 where $\|\bullet\|$ is the Euclidean norm operator.

133 With the assumption of infinitesimal deformation, the strain components
 134 with respect to the global contravariant base can be stated as:

$$\epsilon_{ij} = \frac{1}{2}(\mathbf{x}_{,i} \cdot \mathbf{u}_{,j} + \mathbf{u}_{,i} \cdot \mathbf{x}_{,j}) \quad (4)$$

where \mathbf{u} represents the displacement for the shell deformation. To satisfy the Kirchhoff hypothesis, the displacement is assumed to be of the following form:

$$\mathbf{u}(\xi^1, \xi^2, \xi^3) = \mathbf{v}(\xi^1, \xi^2) + \boldsymbol{\theta}(\xi^1, \xi^2)\xi^3 \quad (5)$$

in which the quadratic and higher order terms are neglected. \mathbf{v} , $\boldsymbol{\theta}$ represent the displacement and rotation in mid-surface, respectively.

Subsequently, plugging Eqs. (1) and (5) into Eq. (4) and neglecting the quadratic terms, the strain components can be rephrased as follows:

$$\begin{aligned} \epsilon_{\alpha\beta} &= \frac{1}{2}(\mathbf{a}_\alpha \cdot \mathbf{v}_{,\beta} + \mathbf{v}_{,\alpha} \cdot \mathbf{a}_\beta) \\ &+ \frac{1}{2}(\mathbf{a}_{3,\alpha} \cdot \mathbf{v}_{,\beta} + \mathbf{v}_{,\alpha} \cdot \mathbf{a}_{3,\beta} + \mathbf{a}_\alpha \cdot \boldsymbol{\theta}_{,\beta} + \boldsymbol{\theta}_{,\alpha} \cdot \mathbf{a}_\beta)\xi^3 \\ &= \varepsilon_{\alpha\beta} + \kappa_{\alpha\beta}\xi^3 \end{aligned} \quad (6a)$$

$$\epsilon_{\alpha 3} = \frac{1}{2}(\mathbf{a}_\alpha \cdot \boldsymbol{\theta} + \mathbf{v}_{,\alpha} \cdot \mathbf{a}_3) + \frac{1}{2}(\mathbf{a}_3 \cdot \boldsymbol{\theta})_{,\alpha}\xi^3 \quad (6b)$$

$$\epsilon_{33} = \mathbf{a}_3 \cdot \boldsymbol{\theta} \quad (6c)$$

where $\varepsilon_{\alpha\beta}$, $\kappa_{\alpha\beta}$ represent membrane and bending strains, respectively, and are given as follows:

$$\varepsilon_{\alpha\beta} = \frac{1}{2}(\mathbf{a}_\alpha \cdot \mathbf{v}_{,\beta} + \mathbf{v}_{,\alpha} \cdot \mathbf{a}_\beta) \quad (7)$$

$$\kappa_{\alpha\beta} = \frac{1}{2}(\mathbf{a}_{3,\alpha} \cdot \mathbf{v}_{,\beta} + \mathbf{v}_{,\alpha} \cdot \mathbf{a}_{3,\beta} + \mathbf{a}_\alpha \cdot \boldsymbol{\theta}_{,\beta} + \boldsymbol{\theta}_{,\alpha} \cdot \mathbf{a}_\beta) \quad (8)$$

In accordance with the Kirchhoff hypothesis, the thickness of shell will not change, and the deformation related with direction of ξ^3 will vanish, i.e. $\epsilon_{3i} = 0$. Thus, the rotation $\boldsymbol{\theta}$ can be rewritten as:

$$\epsilon_{3i} = 0 \Rightarrow \begin{cases} \boldsymbol{\theta} \cdot \mathbf{a}_\alpha + \mathbf{v}_{,\alpha} \cdot \mathbf{a}_3 = 0 \\ \boldsymbol{\theta} \cdot \mathbf{a}_3 = 0 \end{cases} \Rightarrow \boldsymbol{\theta} = -\mathbf{v}_{,\alpha} \cdot \mathbf{a}_3 \mathbf{a}^\alpha \quad (9)$$

where \mathbf{a}^α 's is the in-plane contravariant base vector, $\mathbf{a}^\alpha \cdot \mathbf{a}_\beta = \delta^\alpha_\beta$, δ is the Kronecker delta function. [Substituting The detailed derivation of Eq. 9 can be found in reference \[29\].](#)

[Furthermore, substituting](#) Eq. (9) into Eq. (8) leads to:

$$\kappa_{\alpha\beta} = (\Gamma_{\alpha\beta}^\gamma \mathbf{v}_{,\gamma} - \mathbf{v}_{,\alpha\beta}) \cdot \mathbf{a}_3 = -\mathbf{v}_{,\alpha}|_\beta \cdot \mathbf{a}_3 \quad (10)$$

in which $\Gamma_{\alpha\beta}^\gamma = \mathbf{a}_{\alpha,\beta} \cdot \mathbf{a}^\gamma$ is namely the Christoffel symbol of the second kind, and $\mathbf{v}_{,\alpha}|_\beta$ is the in-plane covariant derivative of $\mathbf{v}_{,\alpha}$, i.e. $\mathbf{v}_{,\alpha}|_\beta = \Gamma_{\alpha\beta}^\gamma \mathbf{v}_{,\gamma} - \mathbf{v}_{,\alpha\beta}$.

2.2. Galerkin weak form for Hu-Washizu principle of complementary energy

In this study, the Hu-Washizu variational principle of complementary energy [30] was adopted for the development of the proposed analytical approach, the

corresponding complementary functional, denoted by Π_C , is listed as follows:

$$\begin{aligned}
& \Pi_C(\varepsilon_{\alpha\beta}, \kappa_{\alpha\beta}, N^{\alpha\beta}, M^{\alpha\beta}) \\
&= \int_{\Omega} \frac{h}{2} \varepsilon_{\alpha\beta} C^{\alpha\beta\gamma\eta} \varepsilon_{\gamma\eta} d\Omega + \int_{\Omega} \frac{h^3}{24} \kappa_{\alpha\beta} C^{\alpha\beta\gamma\eta} \kappa_{\gamma\eta} d\Omega \\
&+ \int_{\Omega} \varepsilon_{\alpha\beta} (N^{\alpha\beta} - h C^{\alpha\beta\gamma\eta} \varepsilon_{\gamma\eta}) d\Omega + \int_{\Omega} \kappa_{\alpha\beta} (M^{\alpha\beta} - \frac{h^3}{12} C^{\alpha\beta\gamma\eta} \kappa_{\gamma\eta}) d\Omega \\
&- \int_{\Gamma_v} \mathbf{T} \cdot \bar{\mathbf{v}} d\Gamma + \int_{\Gamma_{\theta}} M_{\mathbf{nn}} \bar{\theta}_{\mathbf{n}} d\Gamma - (P \mathbf{a}_3 \cdot \bar{\mathbf{v}})_{\mathbf{x} \in C_w}
\end{aligned} \tag{11}$$

where $C^{\alpha\beta\gamma\eta}$'s represent the components of fourth order elasticity tensor with respect to the covariant base and plane stress assumption, and it can be expressed by Young's modulus E , Poisson's ratio ν and the in-plane contravariant metric coefficients $a^{\alpha\beta}$'s, $a^{\alpha\beta} = \mathbf{a}^{\alpha} \cdot \mathbf{a}^{\beta}$, as follows:

$$C^{\alpha\beta\gamma\eta} = \frac{E}{2(1+\nu)} (a^{\alpha\gamma} a^{\beta\eta} + a^{\alpha\eta} a^{\beta\gamma} + \frac{2\nu}{1-\nu} a^{\alpha\beta} a^{\gamma\eta}) \tag{12}$$

and $N^{\alpha\beta}$, $M^{\alpha\beta}$ are the components of membrane and bending stresses given by:

$$N^{\alpha\beta} = h C^{\alpha\beta\gamma\eta} \varepsilon_{\gamma\eta}, \quad M^{\alpha\beta} = \frac{h^3}{12} C^{\alpha\beta\gamma\eta} \kappa_{\gamma\eta} \tag{13}$$

Essential boundaries on the edges and corners denoted by Γ_v , Γ_{θ} and C_v are naturally existed in complementary energy functional, $\bar{\mathbf{v}}$, $\bar{\theta}_{\mathbf{n}}$ are the corresponding prescribed displacement and normal rotation, respectively. \mathbf{T} , $M_{\mathbf{nn}}$ and P can be determined by Euler-Lagrange equations of shell problem [29] as follows:

$$\mathbf{T} = \mathbf{T}_N + \mathbf{T}_M \rightarrow \begin{cases} \mathbf{T}_N = \mathbf{a}_{\alpha} N^{\alpha\beta} n_{\beta} \\ \mathbf{T}_M = (\mathbf{a}_3 M^{\alpha\beta} s_{\alpha} n_{\beta})_{,\gamma} s^{\gamma} + (\mathbf{a}_3 M^{\alpha\beta})_{|\beta} n_{\alpha} \end{cases} \tag{14}$$

$$M_{\mathbf{nn}} = M^{\alpha\beta} n_{\alpha} n_{\beta} \tag{15}$$

$$P = -[[M^{\alpha\beta} s_{\alpha} n_{\beta}]] \tag{16}$$

where $\mathbf{n} = n^{\alpha} \mathbf{a}_{\alpha} = n_{\alpha} \mathbf{a}^{\alpha}$ and $\mathbf{s} = s^{\alpha} \mathbf{a}_{\alpha} = s_{\alpha} \mathbf{a}^{\alpha}$ are the outward normal and tangent directions on boundaries. $[[f]]$ is the jump operator defined by:

$$[[f]]_{\mathbf{x}=\mathbf{x}_c} = \lim_{\epsilon \rightarrow 0^+} (f(\mathbf{x}_c + \epsilon) - f(\mathbf{x}_c - \epsilon)), \mathbf{x}_c \in \Gamma \tag{17}$$

where f is an arbitrary function on Γ .

Moreover, the natural boundary conditions should be applied by Lagrangian multiplier method with displacement \mathbf{v} regarded as multiplier. Thus, then the new complementary energy functional namely Π is given by:

$$\begin{aligned}
& \Pi(\mathbf{v}, \varepsilon_{\alpha\beta}, \kappa_{\alpha\beta}, N^{\alpha\beta}, M^{\alpha\beta}) \\
&= \Pi_C(\varepsilon_{\alpha\beta}, \kappa_{\alpha\beta}, N^{\alpha\beta}, M^{\alpha\beta}) + \int_{\Gamma_M} \theta_{\mathbf{n}} (M_{\mathbf{nn}} - \bar{M}_{\mathbf{nn}}) d\Gamma \\
&- \int_{\Gamma_T} \mathbf{v} \cdot (\mathbf{T} - \bar{\mathbf{T}}) d\Gamma - \mathbf{v} \cdot \mathbf{a}_3 (P - \bar{P})_{\mathbf{x} \in C_P} - \int_{\Omega} \mathbf{v} \cdot (\mathbf{b} - \bar{\mathbf{b}}) d\Omega
\end{aligned} \tag{18}$$

175 where $\bar{\mathbf{T}}$, \bar{M}_{nn} and \bar{P} are the prescribed traction, bending moment and concen-
 176 trated force on edges Γ_T , Γ_M and corner C_P respectively. All the boundaries
 177 meet the following geometric relationships:

$$\begin{cases} \Gamma = \Gamma_v \cup \Gamma_T \cup \Gamma_\theta \cup \Gamma_M, & C = C_v \cup C_P, \\ \Gamma_v \cap \Gamma_T = \Gamma_\theta \cap \Gamma_M = C_v \cap C_P = \emptyset \end{cases} \quad (19)$$

178 and $\bar{\mathbf{b}}$ stands for the prescribed body force in Ω , \mathbf{b} also can be written based on
 179 Euler-Lagrange equations [29] as:

$$\mathbf{b} = \mathbf{b}_N + \mathbf{b}_M \rightarrow \begin{cases} \mathbf{b}_N = (\mathbf{a}_\alpha N^{\alpha\beta})|_\beta \\ \mathbf{b}_M = (\mathbf{a}_3 M^{\alpha\beta})|_{\alpha\beta} \end{cases} \quad (20)$$

180 Introducing a standard variational argument to Eq. (18), $\delta\Pi = 0$, and
 181 considering the arbitrariness of virtual variables, $\delta\mathbf{v}$, $\delta\varepsilon_{\alpha\beta}$, $\delta\kappa_{\alpha\beta}$, $N^{\alpha\beta}$, $M^{\alpha\beta}$
 182 lead to the following weak form:

$$-\int_{\Omega} h\delta\varepsilon_{\alpha\beta} C^{\alpha\beta\gamma\eta} \varepsilon_{\gamma\eta} d\Omega + \int_{\Omega} \delta\varepsilon_{\alpha\beta} N^{\alpha\beta} d\Omega = 0 \quad (21a)$$

$$-\int_{\Omega} \frac{h^3}{12} \delta\kappa_{\alpha\beta} C^{\alpha\beta\gamma\eta} \kappa_{\gamma\eta} d\Omega + \int_{\Omega} \delta\kappa_{\alpha\beta} M^{\alpha\beta} d\Omega = 0 \quad (21b)$$

$$\begin{aligned} \int_{\Omega} \delta N^{\alpha\beta} \varepsilon_{\alpha\beta} d\Omega - \int_{\Gamma} \delta \mathbf{T}_N \cdot \mathbf{v} d\Gamma + \int_{\Omega} \delta \mathbf{b}_N \cdot \mathbf{v} d\Omega \\ + \int_{\Gamma_v} \delta \mathbf{T}_N \cdot \mathbf{v} d\Gamma = \int_{\Gamma_v} \delta \mathbf{T}_N \cdot \bar{\mathbf{v}} d\Gamma \end{aligned} \quad (21c)$$

$$\begin{aligned} \int_{\Omega} \delta M^{\alpha\beta} \kappa_{\alpha\beta} d\Omega - \int_{\Gamma} \delta M_{nn} \theta_n d\Gamma + \int_{\Gamma} \delta \mathbf{T}_M \cdot \mathbf{v} d\Gamma + (\delta P \mathbf{a}_3 \cdot \mathbf{v})_{\mathbf{x} \in C} + \int_{\Omega} \delta \mathbf{b}_M \cdot \mathbf{v} d\Omega \\ + \int_{\Gamma_\theta} \delta M_{nn} \theta_n d\Gamma - \int_{\Gamma_v} \delta \mathbf{T}_M \cdot \mathbf{v} d\Gamma - (\delta P \mathbf{a}_3 \cdot \mathbf{v})_{\mathbf{x} \in C_v} \\ = \int_{\Gamma_\theta} \delta M_{nn} \bar{\theta}_n d\Gamma - \int_{\Gamma_v} \delta \mathbf{T}_M \cdot \bar{\mathbf{v}} d\Gamma - (\delta P \mathbf{a}_3 \cdot \bar{\mathbf{v}})_{\mathbf{x} \in C_v} \end{aligned} \quad (21d)$$

$$\begin{aligned} \int_{\Gamma} \delta \theta_n M_{nn} d\Gamma - \int_{\Gamma} \delta \mathbf{v} \cdot \mathbf{T} d\Gamma - (\delta \mathbf{v} \cdot \mathbf{a}_3 P)_{\mathbf{x} \in C} + \int_{\Omega} \delta \mathbf{v} \cdot \mathbf{b} d\Omega \\ - \int_{\Gamma_\theta} \delta \theta_n M_{nn} d\Gamma + \int_{\Gamma_v} \delta \mathbf{v} \cdot \mathbf{T} d\Gamma + (\delta \mathbf{v} \cdot \mathbf{a}_3 P)_{\mathbf{x} \in C_v} = - \int_{\Gamma_T} \delta \mathbf{v} \cdot \bar{\mathbf{t}} d\Gamma - \int_{\Omega} \delta \mathbf{v} \cdot \bar{\mathbf{b}} d\Omega \end{aligned} \quad (21e)$$

187 where the geometric relationships of Eq. (19) is used herein.

188 **3. Mixed meshfree formulation for modified Hellinger-Reissner weak** 189 **form**

190 *3.1. Reproducing kernel approximation for displacement*

191 This study approximates the displacement by adopting reproducing kernel
192 approximation. As shown in Fig. 2, the mid-surface of the shell Ω is discretized
193 by a set of meshfree nodes $\{\boldsymbol{\xi}_I\}_{I=1}^{n_p}$ in parametric configuration, where n_p is the
194 total number of meshfree nodes. The approximated displacement namely \boldsymbol{v}^h
195 can be expressed as:

$$\boldsymbol{v}(\boldsymbol{\xi}) = \sum_{I=1}^{n_p} \Psi_I(\boldsymbol{\xi}) \boldsymbol{d}_I \quad (22)$$

196 in which Ψ_I and \boldsymbol{d}_I is the shape function and nodal coefficient tensor related by
197 node $\boldsymbol{\xi}_I$. According to reproducing kernel approximation [4], the shape function
198 takes the following form:

$$\Psi_I(\boldsymbol{\xi}) = \boldsymbol{p}^T(\boldsymbol{\xi}) \boldsymbol{c}(\boldsymbol{\xi}) \phi(\boldsymbol{\xi}_I - \boldsymbol{\xi}) \quad (23)$$

199 where \boldsymbol{p} is the basis function vector represented using the following quadratic
200 function as:

$$\boldsymbol{p} = \{1, \xi^1, \xi^2, (\xi^1)^2, \xi^1 \xi^2, (\xi^2)^2\}^T \quad (24)$$

201 The kernel function denoted by ϕ controls the support and smoothness of
202 meshfree shape functions. The quintic B-spline function with square support is
203 used herein as the kernel function:

$$\phi(\boldsymbol{\xi}_I - \boldsymbol{\xi}) = \phi(\hat{s}_1) \phi(\hat{s}_2), \quad \hat{s}_\alpha = \frac{|\xi_I^\alpha - \xi^\alpha|}{s_{\alpha I}} \quad (25)$$

204 with

$$\phi(\hat{s}_\alpha) = \frac{1}{5!} \begin{cases} (3 - 3\hat{s}_\alpha)^5 - 6(2 - 3\hat{s}_\alpha)^5 + 15(1 - 3\hat{s}_\alpha)^5 & \hat{s}_\alpha \leq \frac{1}{3} \\ (3 - 3\hat{s}_\alpha)^5 - 6(2 - 3\hat{s}_\alpha)^5 & \frac{1}{3} < \hat{s}_\alpha \leq \frac{2}{3} \\ (3 - 3\hat{s}_\alpha)^5 & \frac{2}{3} < \hat{s}_\alpha \leq 1 \\ 0 & \hat{s}_\alpha > 1 \end{cases} \quad (26)$$

205 and $s_{\alpha I}$ means the support size of meshfree shape function Ψ_I .

206 The unknown vector \boldsymbol{c} in shape function are determined by the fulfillment
207 of the so-called consistency condition:

$$\sum_{I=1}^{n_p} \Psi_I(\boldsymbol{\xi}) \boldsymbol{p}(\boldsymbol{\xi}_I) = \boldsymbol{p}(\boldsymbol{\xi}) \quad (27)$$

208 or equivalently

$$\sum_{I=1}^{n_p} \Psi_I(\boldsymbol{\xi}) \boldsymbol{p}(\boldsymbol{\xi}_I - \boldsymbol{\xi}) = \boldsymbol{p}(\mathbf{0}) \quad (28)$$

209 Substituting Eq. (22) into (28), yields:

$$\mathbf{A}(\boldsymbol{\xi})\mathbf{c}(\boldsymbol{\xi}) = \mathbf{p}(\mathbf{0}) \quad \Rightarrow \quad \mathbf{c}(\boldsymbol{\xi}) = \mathbf{A}^{-1}(\boldsymbol{\xi})\mathbf{p}(\mathbf{0}) \quad (29)$$

210 where \mathbf{A} is the moment matrix:

$$\mathbf{A}(\boldsymbol{\xi}) = \sum_{I=1}^{n_p} \phi(\boldsymbol{\xi}_I - \boldsymbol{\xi}) \mathbf{p}(\boldsymbol{\xi}_I - \boldsymbol{\xi}) \mathbf{p}^T(\boldsymbol{\xi}_I - \boldsymbol{\xi}) \quad (30)$$

211 Substituting Eq. (29) back into Eq. (22), the expression of meshfree shape
212 function can be written as:

$$\Psi_I(\boldsymbol{\xi}) = \mathbf{p}^T(\boldsymbol{\xi}_I - \boldsymbol{\xi}) \mathbf{A}^{-1}(\boldsymbol{\xi}) \mathbf{p}(\mathbf{0}) \phi(\boldsymbol{\xi}_I - \boldsymbol{\xi}) \quad (31)$$

213 3.2. Reproducing kernel gradient smoothing approximation for effective stress 214 and strain

215 In Galerkin meshfree formulation, the mid-plane of thin shell Ω is split by
216 a set of integration cells Ω_C 's, $\cup_{C=1}^{n_e} \Omega_C \approx \Omega$, as shown in Fig. 2. With the
217 inspiration of reproducing kernel smoothing framework, the Cartesian and co-
218 variant derivatives of displacement, $\mathbf{v}_{,\alpha}$ and $-\mathbf{v}_{,\alpha}|_{\beta}$, in strains $\varepsilon_{\alpha\beta}$, $\kappa_{\alpha\beta}$ are
219 approximated by $(p-1)$ -th order polynomials in each integration cells. In inte-
220 gration cell Ω_C , the approximated derivatives and strains denoted by $\mathbf{v}_{,\alpha}^h$, $\varepsilon_{\alpha\beta}^h$
221 and $-\mathbf{v}_{,\alpha}^h|_{\beta}$, $\kappa_{\alpha\beta}^h$ can be expressed by:

$$\mathbf{v}_{,\alpha}^h(\boldsymbol{\xi}) = \mathbf{q}^T(\boldsymbol{\xi}) \mathbf{d}_{\alpha}^{\varepsilon}, \quad \varepsilon_{\alpha\beta}^h(\boldsymbol{\xi}) = \mathbf{q}^T(\boldsymbol{\xi}) \frac{1}{2} (\mathbf{a}_{\alpha} \cdot \mathbf{d}_{\beta}^{\varepsilon} + \mathbf{a}_{\beta} \cdot \mathbf{d}_{\alpha}^{\varepsilon}) \quad (32)$$

$$-\mathbf{v}_{,\alpha}^h|_{\beta}(\boldsymbol{\xi}) = \mathbf{q}^T(\boldsymbol{\xi}) \mathbf{d}_{\alpha\beta}^{\kappa}, \quad \kappa_{\alpha\beta}^h(\boldsymbol{\xi}) = \mathbf{q}^T(\boldsymbol{\xi}) \mathbf{a}_3 \cdot \mathbf{d}_{\alpha\beta}^{\kappa} \quad (33)$$

223 where \mathbf{q} is the linear polynomial vector and has the following form:

$$\mathbf{q} = \{1, \xi^1, \xi^2\}^T \quad (34)$$

224 and the $\mathbf{d}_{\alpha}^{\varepsilon}$, $\mathbf{d}_{\alpha\beta}^{\kappa}$ are the corresponding coefficient vector tensors. For the con-
225 ciseness, the mixed usage of tensor and vector is introduced in this study. For
226 instance, the component of coefficient tensor vector $\mathbf{d}_{\alpha I}^{\varepsilon}$, $\mathbf{d}_{\alpha}^{\varepsilon} = \{\mathbf{d}_{\alpha I}^{\varepsilon}\}$, is a three
227 dimensional tensor, $\dim \mathbf{d}_{\alpha I}^{\varepsilon} = \dim \mathbf{v}$.

228 In order to meet the integration constraint of thin shell problem, the ap-
229 proximated stresses $N^{\alpha\beta h}$, $M^{\alpha\beta h}$ are assumed to be a similar form with strains,
230 yields:

$$N^{\alpha\beta h}(\boldsymbol{\xi}) = \mathbf{q}^T(\boldsymbol{\xi}) \mathbf{a}^{\alpha} \cdot \mathbf{d}_N^{\beta}, \quad \mathbf{a}_{\alpha} N^{\alpha\beta h}(\boldsymbol{\xi}) = \mathbf{q}^T(\boldsymbol{\xi}) \mathbf{d}_N^{\beta} \quad (35)$$

$$M^{\alpha\beta h}(\boldsymbol{\xi}) = \mathbf{q}^T(\boldsymbol{\xi}) \mathbf{a}_3 \cdot \mathbf{d}_M^{\alpha\beta}, \quad \mathbf{a}_3 M^{\alpha\beta h}(\boldsymbol{\xi}) = \mathbf{q}^T(\boldsymbol{\xi}) \mathbf{d}_M^{\alpha\beta} \quad (36)$$

232 substituting the approximations of Eqs. (22), (32), (33), (35), (36) into Eqs.
233 (21c), (21d) can express $\mathbf{d}_{\beta}^{\varepsilon}$ and $\mathbf{d}_{\alpha\beta}^{\kappa}$ by \mathbf{d} as:

$$\mathbf{d}_{\beta}^{\varepsilon} = \mathbf{G}^{-1} \left(\sum_{I=1}^{n_p} (\tilde{\mathbf{g}}_{\beta I} - \bar{\mathbf{g}}_{\beta I}) \mathbf{d}_I + \hat{\mathbf{g}}_{\beta} \right) \quad (37)$$

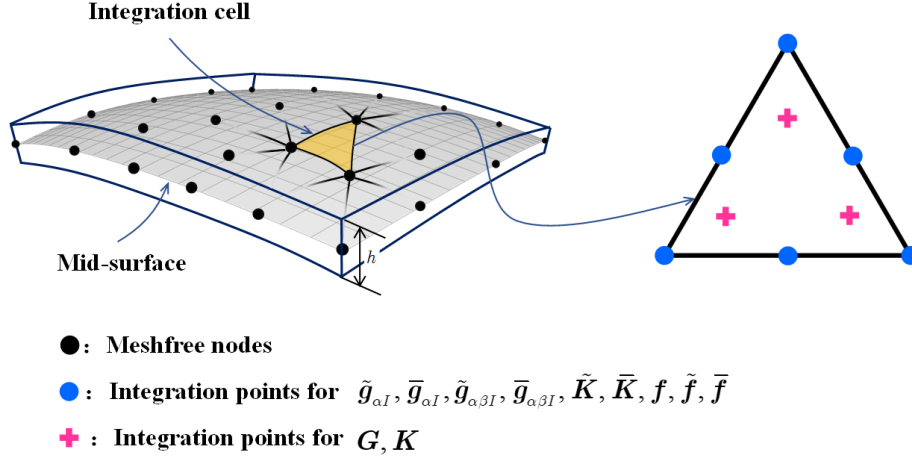


Figure 2: Integration scheme for Hu-Washizu weak form.

234

$$d_{\alpha\beta}^{\kappa} = G^{-1} \left(\sum_{I=1}^{n_p} (\tilde{g}_{\alpha\beta I} - \bar{g}_{\alpha\beta I}) d_I + \hat{g}_{\alpha\beta} \right) \quad (38)$$

235 with

$$G = \int_{\Omega_C} q^T q d\Omega \quad (39)$$

236

$$\tilde{g}_{\beta I} = \int_{\Gamma_C} \Psi_I q n_{\beta} d\Gamma - \int_{\Omega_C} \Psi_I q_{|\beta} d\Omega \quad (40a)$$

$$\bar{g}_{\beta I} = \int_{\Gamma_C \cap \Gamma_v} \Psi_I q n_{\beta} d\Gamma \quad (40b)$$

$$\hat{g}_{\beta} = \int_{\Gamma_C \cap \Gamma_v} q n_{\beta} \bar{v} d\Gamma \quad (40c)$$

237

$$\begin{aligned} \tilde{g}_{\alpha\beta I} = & \int_{\Gamma_C} \Psi_{I,\gamma} n^{\gamma} q n_{\alpha} n_{\beta} d\Gamma - \int_{\Gamma_C} \Psi_I (q_{|\beta} n_{\alpha} + (q s_{\alpha} n_{\beta})_{,\gamma} s^{\gamma}) d\Gamma \\ & + [[\Psi_I q s_{\alpha} n_{\beta}]]_{\mathbf{x} \in C_C} - \int_{\Omega_C} \Psi q_{,\alpha|\beta} d\Omega \end{aligned} \quad (41a)$$

$$\begin{aligned} \bar{g}_{\alpha\beta I} = & \int_{\Gamma_C \cap \Gamma_{\theta}} \Psi_{I,\gamma} n^{\gamma} q n_{\alpha} n_{\beta} d\Gamma - \int_{\Gamma_C \cap \Gamma_v} \Psi_I (q_{|\beta} n_{\alpha} + (q s_{\alpha} n_{\beta})_{,\gamma} s^{\gamma}) d\Gamma \\ & + [[\Psi_I q s_{\alpha} n_{\beta}]]_{\mathbf{x} \in C_C \cap C_v} \end{aligned} \quad (41b)$$

$$\begin{aligned} \hat{g}_{\alpha\beta} = & \int_{\Gamma_C \cap \Gamma_{\theta}} q n_{\alpha} n_{\beta} a_3 \bar{\theta}_{\mathbf{n}} d\Gamma - \int_{\Gamma_C \cap \Gamma_v} (q_{|\beta} n_{\alpha} + (q s_{\alpha} n_{\beta})_{,\gamma} s^{\gamma}) \bar{v} d\Gamma \\ & + [[q s_{\alpha} n_{\beta} \bar{v}]]_{\mathbf{x} \in C_C \cap C_v} \end{aligned} \quad (41c)$$

where evaluations of $\mathbf{q}_{|\beta}$, $\mathbf{q}_{,\alpha|\beta}$ are detail in Appendix A. Further plugging Eqs. (37) and (38) back into Eqs. (32) and (33) respectively gives the final expression of $\mathbf{v}_{,\alpha}^h$, $\varepsilon_{\alpha\beta}^h$ and $-\mathbf{v}_{,\alpha\beta}^h$, $\kappa_{\alpha\beta}^h$ as:

$$\mathbf{v}_{,\alpha}^h = \sum_{I=1}^{n_p} (\tilde{\Psi}_{I,\alpha} - \bar{\Psi}_{I,\alpha}) \mathbf{d}_I + \mathbf{q}^T \mathbf{G}^{-1} \hat{\mathbf{g}}_\alpha \quad (42a)$$

$$\begin{aligned} \varepsilon_{\alpha\beta}^h &= \sum_{I=1}^{n_p} \frac{1}{2} (\mathbf{a}_\alpha \tilde{\Psi}_{I,\beta} + \mathbf{a}_\beta \tilde{\Psi}_{I,\alpha}) \cdot \mathbf{d}_I - \sum_{I=1}^{n_p} \frac{1}{2} (\mathbf{a}_\alpha \bar{\Psi}_{I,\beta} + \mathbf{a}_\beta \bar{\Psi}_{I,\alpha}) \cdot \mathbf{d}_I \\ &\quad + \mathbf{q}^T \mathbf{G}^{-1} \frac{1}{2} (\mathbf{a}_\alpha \cdot \hat{\mathbf{g}}_\beta + \mathbf{a}_\beta \cdot \hat{\mathbf{g}}_\alpha) \\ &= \tilde{\varepsilon}_{\alpha\beta}^h - \bar{\varepsilon}_{\alpha\beta}^h + \hat{\varepsilon}_{\alpha\beta}^h \end{aligned} \quad (42b)$$

$$-\mathbf{v}_{,\alpha\beta}^h = \sum_{I=1}^{n_p} (\tilde{\Psi}_{I,\alpha\beta} - \bar{\Psi}_{I,\alpha\beta}) \mathbf{d}_I + \mathbf{q}^T \mathbf{G}^{-1} \hat{\mathbf{g}}_{\alpha\beta} \quad (43a)$$

$$\begin{aligned} \kappa_{\alpha\beta}^h &= \sum_{I=1}^{n_p} \tilde{\Psi}_{I,\alpha\beta} \mathbf{a}_3 \cdot \mathbf{d}_I - \sum_{I=1}^{n_p} \bar{\Psi}_{I,\alpha\beta} \mathbf{a}_3 \cdot \mathbf{d}_I + \mathbf{q}^T \mathbf{G}^{-1} \mathbf{a}_3 \cdot \hat{\mathbf{g}}_{\alpha\beta} \\ &= \tilde{\kappa}_{\alpha\beta}^h - \bar{\kappa}_{\alpha\beta}^h + \hat{\kappa}_{\alpha\beta}^h \end{aligned} \quad (43b)$$

with

$$\begin{cases} \tilde{\varepsilon}_{\alpha\beta}^h = \sum_{I=1}^{n_p} \frac{1}{2} (\mathbf{a}_\alpha \tilde{\Psi}_{I,\beta} + \mathbf{a}_\beta \tilde{\Psi}_{I,\alpha}) \cdot \mathbf{d}_I = \sum_{I=1}^{n_p} \tilde{\varepsilon}_{\alpha\beta I} \cdot \mathbf{d}_I \\ \bar{\varepsilon}_{\alpha\beta}^h = \sum_{I=1}^{n_p} \frac{1}{2} (\mathbf{a}_\alpha \bar{\Psi}_{I,\beta} + \mathbf{a}_\beta \bar{\Psi}_{I,\alpha}) \cdot \mathbf{d}_I = \sum_{I=1}^{n_p} \bar{\varepsilon}_{\alpha\beta I} \cdot \mathbf{d}_I \\ \hat{\varepsilon}_{\alpha\beta}^h = \mathbf{q}^T \mathbf{G}^{-1} \frac{1}{2} (\mathbf{a}_\alpha \cdot \hat{\mathbf{g}}_\beta + \mathbf{a}_\beta \cdot \hat{\mathbf{g}}_\alpha) \end{cases} \quad (44)$$

$$\begin{cases} \tilde{\Psi}_{I,\alpha}(\boldsymbol{\xi}) = \mathbf{q}^T(\boldsymbol{\xi}) \mathbf{G}^{-1} \tilde{\mathbf{g}}_{\alpha I} \\ \bar{\Psi}_{I,\alpha}(\boldsymbol{\xi}) = \mathbf{q}^T(\boldsymbol{\xi}) \mathbf{G}^{-1} \bar{\mathbf{g}}_{\alpha I} \\ \tilde{\varepsilon}_{\alpha\beta I} = \frac{1}{2} (\mathbf{a}_\alpha \tilde{\Psi}_{I,\beta} + \mathbf{a}_\beta \tilde{\Psi}_{I,\alpha}) \\ \bar{\varepsilon}_{\alpha\beta I} = \frac{1}{2} (\mathbf{a}_\alpha \bar{\Psi}_{I,\beta} + \mathbf{a}_\beta \bar{\Psi}_{I,\alpha}) \end{cases} \quad (45)$$

$$\begin{cases} \tilde{\kappa}_{\alpha\beta}^h = \sum_{I=1}^{n_p} \tilde{\Psi}_{I,\alpha\beta} \mathbf{a}_3 \cdot \mathbf{d}_I = \sum_{I=1}^{n_p} \tilde{\kappa}_{\alpha\beta I} \cdot \mathbf{d}_I \\ \bar{\kappa}_{\alpha\beta}^h = \sum_{I=1}^{n_p} \bar{\Psi}_{I,\alpha\beta} \mathbf{a}_3 \cdot \mathbf{d}_I = \sum_{I=1}^{n_p} \bar{\kappa}_{\alpha\beta I} \cdot \mathbf{d}_I \\ \hat{\kappa}_{\alpha\beta}^h = \mathbf{q}^T \mathbf{G}^{-1} \mathbf{a}_3 \cdot \hat{\mathbf{g}}_{\alpha\beta} \end{cases} \quad (46)$$

$$\begin{cases} \tilde{\Psi}_{I,\alpha\beta}(\boldsymbol{\xi}) = \mathbf{q}^T(\boldsymbol{\xi})\mathbf{G}^{-1}\tilde{\mathbf{g}}_{\alpha\beta I} \\ \bar{\Psi}_{I,\alpha\beta}(\boldsymbol{\xi}) = \mathbf{q}^T(\boldsymbol{\xi})\mathbf{G}^{-1}\tilde{\mathbf{g}}_{\alpha\beta I} \\ \tilde{\boldsymbol{\kappa}}_{\alpha\beta I} = \tilde{\Psi}_{I,\alpha\beta}\mathbf{a}_3 \\ \bar{\boldsymbol{\kappa}}_{\alpha\beta I} = \bar{\Psi}_{I,\alpha\beta}\mathbf{a}_3 \end{cases} \quad (47)$$

248 It has to be noted that, referring to reproducing kernel gradient smoothing
 249 framework [25], $\tilde{\Psi}_{I,\alpha}$, $\tilde{\Psi}_{I,\alpha\beta}$ are actually the first and second order smoothed
 250 gradients in curvilinear coordinates. $\tilde{\mathbf{g}}_{\alpha I}$ and $\tilde{\mathbf{g}}_{\alpha\beta I}$ are the right hand side in-
 251 tegration constraints for first and second order gradients, then this formulation
 252 can meet the variational consistency for the second order polynomials. It should
 253 be known that, in curved model, the variational consistency for non-polynomial
 254 functions, like trigonometric functions, should be required for the polynomial so-
 255 lution. Even with high order variational consistency, the proposed formulation
 256 can not exactly reproduce the solution spanned by basis functions. However,
 257 the accuracy of reproducing kernel smoothed gradients is still better than tradi-
 258 tional meshfree formulation. Numerical examples in the section below will pro-
 259 vide better evidence to prove the accuracy of the reproducing kernel smoothed
 260 gradients.

261 **4. Naturally variational enforcement for essential boundary condi-**
 262 **tions**

263 *4.1. Discrete equilibrium equations*

264 With the approximated effective stresses and strains, the last equation of
 265 weak form Eq. (21e) becomes:

$$-\sum_{C=1}^{n_e} \sum_{I=1}^{n_p} \delta \mathbf{d}_I \cdot \left((\tilde{\mathbf{g}}_{\alpha I}^T - \bar{\mathbf{g}}_{\alpha I}^T) \mathbf{d}_N^\alpha + (\tilde{\mathbf{g}}_{\alpha \beta I}^T - \bar{\mathbf{g}}_{\alpha \beta I}^T) \mathbf{d}_M^{\alpha \beta} \right) = -\sum_{I=1}^{n_p} \delta \mathbf{d}_I \cdot \mathbf{f}_I \quad (48)$$

266 where \mathbf{f}_I 's are the components of the traditional force vector:

$$\mathbf{f}_I = \int_{\Gamma_t} \Psi_I \bar{\mathbf{t}} d\Gamma - \int_{\Gamma_M} \Psi_{I,\gamma} n^\gamma \bar{M}_{nn} d\Gamma + [[\Psi_I \mathbf{a}_3 \bar{P}]]_{\mathbf{x} \in C_P} + \int_{\Omega} \Psi_I \bar{\mathbf{b}} d\Omega \quad (49)$$

267 The left side of Eq. (48) can be simplified using the following steps. For clarity,
 268 the derivation of first term in Eq. (48) taken as an example is given by:

$$\begin{aligned} \sum_{I=1}^{n_p} \delta \mathbf{d}_I \cdot \tilde{\mathbf{g}}_{\alpha I}^T \mathbf{d}_N^\alpha &= \sum_{I=1}^{n_p} \delta \mathbf{d}_I \cdot (\mathbf{G}^{-1} \tilde{\mathbf{g}}_{\alpha I})^T \mathbf{G} \mathbf{d}_N^\alpha \\ &= \int_{\Omega_C} \sum_{I=1}^{n_p} \delta \mathbf{d}_I \cdot (\mathbf{q}^T \mathbf{G}^{-1} \tilde{\mathbf{g}}_{\alpha I})^T \mathbf{q}^T \mathbf{d}_N^\alpha d\Omega \\ &= \int_{\Omega_C} \sum_{I=1}^{n_p} \delta \mathbf{d}_I \cdot \mathbf{a}_\beta (\mathbf{q}^T \mathbf{G}^{-1} \tilde{\mathbf{g}}_{\alpha I})^T N^{\alpha \beta h} d\Omega \\ &= \int_{\Omega_C} \delta \tilde{\varepsilon}_{\alpha \beta}^h N^{\alpha \beta h} d\Omega \end{aligned} \quad (50)$$

269 following the above procedure and including the weak form of Eqs. (21a), (21b),
 270 the left side of Eq. (48) in Ω_C becomes:

$$\begin{aligned}
 & \sum_{I=1}^{n_p} \delta \mathbf{d}_I \cdot \left((\tilde{\mathbf{g}}_{\alpha I}^T - \bar{\mathbf{g}}_{\alpha I}^T) \mathbf{d}_N^\alpha + (\tilde{\mathbf{g}}_{\alpha \beta I}^T - \bar{\mathbf{g}}_{\alpha \beta I}^T) \mathbf{d}_M^{\alpha \beta} \right) \\
 &= \int_{\Omega_C} ((\delta \tilde{\varepsilon}_{\alpha \beta}^h - \delta \bar{\varepsilon}_{\alpha \beta}^h) N^{\alpha \beta h} + (\delta \tilde{\kappa}_{\alpha \beta}^h - \delta \bar{\kappa}_{\alpha \beta}^h) M^{\alpha \beta h}) d\Omega \\
 &= \int_{\Omega_C} (\delta \tilde{\varepsilon}_{\alpha \beta}^h - \delta \bar{\varepsilon}_{\alpha \beta}^h) h C^{\alpha \beta \gamma \eta} \varepsilon_{\gamma \eta}^h + (\delta \tilde{\kappa}_{\alpha \beta}^h - \delta \bar{\kappa}_{\alpha \beta}^h) \frac{h^3}{12} C^{\alpha \beta \gamma \eta} \kappa_{\gamma \eta}^h \\
 &= \int_{\Omega_C} \delta \tilde{\varepsilon}_{\alpha \beta}^h h C^{\alpha \beta \gamma \eta} \varepsilon_{\gamma \eta}^h d\Omega + \int_{\Omega_C} \delta \tilde{\kappa}_{\alpha \beta}^h \frac{h^3}{12} C^{\alpha \beta \gamma \eta} \kappa_{\gamma \eta}^h d\Omega \\
 &\quad - \int_{\Omega_C} \delta \bar{\varepsilon}_{\alpha \beta}^h h C^{\alpha \beta \gamma \eta} \varepsilon_{\gamma \eta}^h d\Omega - \int_{\Omega_C} \delta \bar{\kappa}_{\alpha \beta}^h h C^{\alpha \beta \gamma \eta} \kappa_{\gamma \eta}^h d\Omega \\
 &\quad - \int_{\Omega_C} \delta \tilde{\kappa}_{\alpha \beta}^h \frac{h^3}{12} C^{\alpha \beta \gamma \eta} \bar{\kappa}_{\gamma \eta}^h d\Omega - \int_{\Omega_C} \delta \bar{\kappa}_{\alpha \beta}^h \frac{h^3}{12} C^{\alpha \beta \gamma \eta} \tilde{\kappa}_{\gamma \eta}^h d\Omega \\
 &\quad + \int_{\Omega_C} \delta \bar{\varepsilon}_{\alpha \beta}^h h C^{\alpha \beta \gamma \eta} \varepsilon_{\gamma \eta}^h d\Omega + \int_{\Omega_C} \delta \bar{\kappa}_{\alpha \beta}^h \frac{h^3}{12} C^{\alpha \beta \gamma \eta} \bar{\kappa}_{\gamma \eta}^h d\Omega \\
 &\quad + \int_{\Omega_C} (\delta \tilde{\varepsilon}_{\alpha \beta}^h - \delta \bar{\varepsilon}_{\alpha \beta}^h) h C^{\alpha \beta \gamma \eta} \varepsilon_{\gamma \eta}^h d\Omega + \int_{\Omega_C} (\delta \tilde{\kappa}_{\alpha \beta}^h - \delta \bar{\kappa}_{\alpha \beta}^h) \frac{h^3}{12} C^{\alpha \beta \gamma \eta} \kappa_{\gamma \eta}^h d\Omega
 \end{aligned} \tag{51}$$

271 on further substituting Eqs. (44) and (46) into above equation gives the final
 272 discrete equilibrium equations, respectively:

$$(\mathbf{K} + \tilde{\mathbf{K}} + \bar{\mathbf{K}}) \mathbf{d} = \mathbf{f} + \tilde{\mathbf{f}} + \bar{\mathbf{f}} \tag{52}$$

273 where

$$\mathbf{K}_{IJ} = \int_{\Omega} \tilde{\varepsilon}_{\alpha \beta I} h C^{\alpha \beta \gamma \eta} \tilde{\varepsilon}_{\gamma \eta J} d\Omega + \int_{\Omega} \tilde{\kappa}_{\alpha \beta I} \frac{h^3}{12} C^{\alpha \beta \gamma \eta} \tilde{\kappa}_{\alpha \beta J} d\Omega \tag{53}$$

274

$$\begin{aligned}
 \tilde{\mathbf{K}}_{IJ} &= - \int_{\Gamma_v} (\Psi_I \tilde{\mathbf{T}}_{NJ} + \tilde{\mathbf{T}}_{NJ} \Psi_J) d\Gamma \\
 &\quad + \int_{\Gamma_\theta} (\Psi_{I,\gamma} n^\gamma \mathbf{a}_3 \tilde{\mathbf{M}}_{nnJ} + \mathbf{a}_3 \tilde{\mathbf{M}}_{nnI} \Psi_{J,\gamma} n^\gamma) d\Gamma
 \end{aligned} \tag{54a}$$

$$\begin{aligned}
 &\quad + ([[\Psi_I \mathbf{a}_3 \tilde{\mathbf{P}}_J]] + [[\tilde{\mathbf{P}}_I \mathbf{a}_3 \Psi_J]])_{\mathbf{x} \in C_v} \\
 \tilde{\mathbf{f}}_I &= - \int_{\Gamma_v} \tilde{\mathbf{T}}_{NI} \cdot \bar{\mathbf{v}} d\Gamma + \int_{\Gamma_\theta} \tilde{\mathbf{M}}_{nnI} \bar{\theta}_n d\Gamma + [[\tilde{\mathbf{P}}_I \mathbf{a}_3 \cdot \bar{\mathbf{v}}]]_{\mathbf{x} \in C_v}
 \end{aligned} \tag{54b}$$

275

$$\bar{\mathbf{K}}_{IJ} = - \int_{\Gamma_v} \bar{\mathbf{T}}_{MI} \Psi_J d\Gamma + \int_{\Gamma_\theta} \mathbf{a}_3 \bar{\mathbf{M}}_{nnI} \Psi_{J,\gamma} n^\gamma d\Gamma + [[\bar{\mathbf{P}}_I \mathbf{a}_3 \Psi_J]]_{\mathbf{x} \in C_v} \tag{55a}$$

$$\bar{\mathbf{f}}_I = - \int_{\Gamma_v} \bar{\mathbf{T}}_{MI} \cdot \bar{\mathbf{v}} d\Gamma + \int_{\Gamma_\theta} \bar{\mathbf{M}}_{nnI} \bar{\theta}_n d\Gamma + [[\bar{\mathbf{P}}_I \mathbf{a}_3 \cdot \bar{\mathbf{v}}]]_{\mathbf{x} \in C_v} \tag{55b}$$

276 The detailed derivations of Eqs (53)-(55) are listed in the Appendix B. As
 277 shown in these equations, Eq. (53) is the conventional stiffness matrix evaluated
 278 by smoothed gradients $\tilde{\Psi}_{I,\alpha}$, $\tilde{\Psi}_{I,\alpha}|_\beta$, and the Eqs. (54) and (55) contribute for
 279 the enforcement of essential boundary. It should be mentioned that, in accor-
 280 dance with reproducing kernel smoothed gradient framework, the integration
 281 scheme of Eqs. (53-55) should be aligned with the those used in the construc-
 282 tion of smoothed gradients. The integration scheme used for proposed method
 283 is shown in Fig. 2, in which the total number of the blue circular integration
 284 points has been optimized from a global point of view, aiming to reduce the com-
 285 putation of traditional meshfree shape functions and its first order derivatives.
 286 In contrast, for assembly stiffness matrix \mathbf{K} , the low order Gauss integration
 287 rule is suitable to ensure the accuracy due to the inherently variational consis-
 288 tency in smoothed gradients. The detailed positions and weight of integration
 289 points and the efficiency demonstration of this optimized integration scheme
 290 can be found in [25, 31] With a close look at Eqs. (54) and (55), the proposed
 291 approach for enforcing essential boundary conditions show an identical struc-
 292 ture with traditional Nitsche's method, both have the consistent and stabilized
 293 terms. So, the next subsection will review the Nitsche's method and compare
 294 it with the proposed method.

295 4.2. Comparison with Nitsche's method

296 The Nitsche's method for enforcing essential boundaries can be regarded as a
 297 combination of Lagrangian multiplier method and penalty method, in which the
 298 Lagrangian multiplier is represented by the approximated displacement. The
 299 corresponding total potential energy functional Π_P is given by:

$$\begin{aligned}
 \Pi_P(\mathbf{v}) = & \int_{\Omega} \frac{1}{2} \varepsilon_{\alpha\beta} N^{\alpha\beta} d\Omega + \int_{\Omega} \frac{1}{2} \kappa_{\alpha\beta} M^{\alpha\beta} d\Omega \\
 & - \int_{\Gamma_t} \mathbf{v} \cdot \bar{\mathbf{t}} d\Gamma + \int_{\Gamma_M} \mathbf{v}_{,\gamma} n^\gamma \mathbf{a}_3 M_{nn} d\Gamma + (\mathbf{v} \cdot \mathbf{a}_3 P)_{\mathbf{x} \in C_P} - \int_{\Omega} \mathbf{v} \cdot \bar{\mathbf{b}} d\Omega \\
 & - \underbrace{\int_{\Gamma_v} \mathbf{t} \cdot (\mathbf{v} - \bar{\mathbf{v}}) d\Gamma + \int_{\Gamma_\theta} M_{nn} (\theta_n - \bar{\theta}_n) d\Gamma + (P \mathbf{a}_3 \cdot (\mathbf{v} - \bar{\mathbf{v}}))_{\mathbf{x} \in C_v}}_{\text{consistent term}} \\
 & + \underbrace{\frac{\alpha_v}{2} \int_{\Gamma_v} \mathbf{v} \cdot \mathbf{v} d\Gamma + \frac{\alpha_\theta}{2} \int_{\Gamma_\theta} \theta_n^2 d\Gamma + \frac{\alpha_C}{2} (\mathbf{v} \cdot \mathbf{v})_{\mathbf{x} \in C_v}}_{\text{stabilized term}}
 \end{aligned} \tag{56}$$

300 where the consistent term generated from the Lagrangian multiplier method
 301 contributes to enforce the essential boundary, and meet the variational con-
 302 sistency condition. However, the consistent term can not always ensure the
 303 coercivity of stiffness, so the penalty method is introduced to serve as a sta-
 304 bilized term. With a standard variational argument, the corresponding weak

form can be stated as:

$$\begin{aligned}
\delta\Pi_P(\mathbf{v}) &= \int_{\Omega} \delta\varepsilon_{\alpha\beta} N^{\alpha\beta} d\Omega + \int_{\Omega} \delta\kappa_{\alpha\beta} M^{\alpha\beta} d\Omega \\
&\quad - \int_{\Gamma_t} \delta\mathbf{v} \cdot \bar{\mathbf{t}} d\Gamma + \int_{\Gamma_M} \delta\mathbf{v}_{,\gamma} n^{\gamma} \mathbf{a}_3 M_{nn} d\Gamma + (\delta\mathbf{v} \cdot \mathbf{a}_3 P)_{\mathbf{x} \in C_P} - \int_{\Omega} \delta\mathbf{v} \cdot \bar{\mathbf{b}} d\Omega \\
&\quad - \int_{\Gamma_v} \delta\mathbf{v} \cdot \mathbf{t} d\Gamma + \int_{\Gamma_{\theta}} \delta\theta_{\mathbf{n}} M_{nn} d\Gamma + (\mathbf{v} \cdot \mathbf{a}_3 P)_{\mathbf{x} \in C_v} \\
&\quad - \int_{\Gamma_v} \delta\mathbf{t} \cdot (\mathbf{v} - \bar{\mathbf{v}}) d\Gamma + \int_{\Gamma_{\theta}} \delta M_{nn} (\theta_{\mathbf{n}} - \bar{\theta}_{\mathbf{n}}) d\Gamma + (\delta P \mathbf{a}_3 \cdot (\mathbf{v} - \bar{\mathbf{v}}))_{\mathbf{x} \in C_v} \\
&\quad + \alpha_v \int_{\Gamma_v} \delta\mathbf{v} \cdot \mathbf{v} d\Gamma + \alpha_{\theta} \int_{\Gamma_{\theta}} \delta\theta_{\mathbf{n}} \theta_{\mathbf{n}} d\Gamma + \alpha_C (\delta\mathbf{v} \cdot \mathbf{v})_{\mathbf{x} \in C_v} \\
&= 0
\end{aligned} \tag{57}$$

in which α_v , α_{θ} and α_C represent experimental artificial parameters. Further invoking the conventional reproducing kernel approximation of Eq. (22) leads to the following discrete equilibrium equations:

$$\sum_{J=1}^{n_p} (\mathbf{K}_{IJ} + \mathbf{K}_{IJ}^c + \mathbf{K}_{IJ}^s) \mathbf{d}_J = \mathbf{f}_I + \mathbf{f}^c + \mathbf{f}^s \tag{58}$$

where the stiffness \mathbf{K}_{IJ} is identical with Eq. (53). \mathbf{K}_{IJ}^c and \mathbf{K}_{IJ}^s are the stiffness matrices for consistent and stabilized terms, respectively, and have the following form:

$$\begin{aligned}
\mathbf{K}_{IJ}^c &= - \int_{\Gamma_v} (\Psi_I \mathbf{T}_{NJ} + \mathbf{T}_{NJ} \Psi_J) d\Gamma \\
&\quad + \int_{\Gamma_{\theta}} (\Psi_{I,\gamma} n^{\gamma} \mathbf{a}_3 \mathbf{M}_{nnJ} + \mathbf{a}_3 \mathbf{M}_{nnI} \Psi_{I,\gamma} n^{\gamma}) d\Gamma \\
&\quad + ([[\Psi_I \mathbf{a}_3 \mathbf{P}_J]] + [[\mathbf{P}_I \mathbf{a}_3 \Psi_J]])_{\mathbf{x} \in C_v}
\end{aligned} \tag{59a}$$

$$\mathbf{f}_I^c = - \int_{\Gamma_v} \mathbf{T}_I \cdot \bar{\mathbf{v}} d\Gamma + \int_{\Gamma_{\theta}} \mathbf{M}_{nnI} \bar{\theta}_{\mathbf{n}} d\Gamma + [[\mathbf{P}_I \mathbf{a}_3 \cdot \bar{\mathbf{v}}]]_{\mathbf{x} \in C_v} \tag{59b}$$

312

$$\mathbf{K}_{IJ}^s = \alpha_v \int_{\Gamma_v} \Psi_I \Psi_J \mathbf{1} d\Gamma + \alpha_{\theta} \int_{\Gamma_{\theta}} \Psi_{I,\eta} n^{\eta} \mathbf{a}_3 \mathbf{a}_3 n^{\gamma} \Psi_{J,\gamma} d\Gamma + \alpha_C [[\Psi_I \mathbf{a}_3 \mathbf{a}_3 \Psi_J]]_{\mathbf{x} \in C_v} \tag{60a}$$

$$\mathbf{f}_I^s = \alpha_v \int_{\Gamma_v} \Psi_I \bar{\mathbf{v}} d\Gamma + \alpha_{\theta} \int_{\Gamma_{\theta}} \Psi_{I,\eta} n^{\eta} \mathbf{a}_3 \bar{\theta}_{\mathbf{n}} d\Gamma + \alpha_C [[\Psi_I \mathbf{a}_3 \mathbf{a}_3 \cdot \bar{\mathbf{v}}]]_{\mathbf{x} \in C_v} \tag{60b}$$

On comparing with the consistent terms of Eqs. (54) and (59), the expressions were almost identical, the major difference is that the higher order derivatives of shape functions have been replaced by smoothed gradients. Owing to

316 the reproducing kernel framework, the construction of smoothed gradients only
317 concerned about the computation of traditional meshfree shape functions and
318 their first order derivatives, which avoid the costly computation of higher order
319 derivatives. Moreover, the stabilized terms in Eq. (60) employs the penalty
320 method to ensure the coercivity of stiffness. In contrast, the stabilized term of
321 Eq. (55) naturally exists in its weak form, and can stabilize the result without
322 considering any artificial parameters.

323 5. Numerical examples

324 The suggested method, which uses Nitsche's method, the consistent repro-
 325 ducing kernel gradient smoothing integration scheme (RKGSI), and the non-
 326 consistent Gauss integration scheme (GI) with penalty method, as well as the
 327 proposed Hu-Washizu formulation (HW) to enforce the necessary boundary con-
 328 ditions, is validated in this section through several examples. A normalized
 329 support size of 2.5 is used for all the methods to ensure the requirement of
 330 quadratic base meshfree approximation. To eliminate the influence of integra-
 331 tion, the Gauss integration scheme uses 6 Gauss points for domain integration
 332 and 3 points for boundary integration, so as to maintain the same integration
 333 accuracy between domain and boundaries. Moreover, the number of integra-
 334 tion points are identical between the Gauss and RKGSI schemes. The error
 335 estimates of displacement (L_2 -Error) and energy (H_e -Error) is used here:

$$\begin{aligned}
 L_2\text{-Error} &= \frac{\sqrt{\int_{\Omega} (\mathbf{v} - \mathbf{v}^h) \cdot (\mathbf{v} - \mathbf{v}^h) d\Omega}}{\sqrt{\mathbf{v} \cdot \mathbf{v}}} \\
 H_e\text{-Error} &= \frac{\sqrt{\int_{\Omega} \left((\varepsilon_{\alpha\beta} - \varepsilon_{\alpha\beta}^h)(N^{\alpha\beta} - N^{\alpha\beta h}) + \int_{\Omega} (\kappa_{\alpha\beta} - \kappa_{\alpha\beta}^h)(M^{\alpha\beta} - M^{\alpha\beta h}) \right) d\Omega}}{\sqrt{\int_{\Omega} (\varepsilon_{\alpha\beta} N^{\alpha\beta} + \kappa_{\alpha\beta} M^{\alpha\beta}) d\Omega}}
 \end{aligned}
 \tag{61}$$

336 5.1. Patch tests

337 The linear and quadratic patch tests for flat and curved thin shells are firstly
 338 studied to verify the variational consistency of the proposed method. As shown
 339 in Fig. 3, the flat and curved models are depicted by an identical parametric
 340 domain $\Omega = (0, 1) \otimes (0, 1)$, where the cylindrical coordinate system with radius
 341 $R = 1$ is employed to describe the curved model, and the whole domain Ω
 342 is discretized by the 165 meshfree nodes. The artificial parameters of $\alpha_v =$
 343 α_θ, α_c . All the boundaries are enforced as essential boundary conditions with
 344 the following manufactured exact solution:

$$\mathbf{v} = \begin{Bmatrix} (\xi^1 + 2\xi^2)^n \\ (3\xi^1 + 4\xi^2)^n \\ (5\xi^1 + 6\xi^2)^n \end{Bmatrix}, \quad n = \begin{cases} 1 & \text{Linear patch test} \\ 2 & \text{Quadratic patch test} \end{cases}
 \tag{62}$$

345 Table 1 lists the L_2 - and H_e -Error results of patch test with flat model, where
 346 the RKGSI scheme with variational consistent essential boundary enforcement,
 347 i.e. RKGSI-Nitsche and RKGSI-HW, can pass the linear and quadratic patch
 348 test. In contrast, the RKGSI-Penalty cannot pass the patch test since the
 349 Penalty method is unable to ensure the variational consistency. Due to the
 350 loss of variational consistency condition, even with Nitsche's method, Gauss
 351 meshfree formulations show noticeable errors. Table 2 shows the results for
 352 curved model, which indicated that all the considered methods cannot pass the
 353 patch test. This is mainly because the proposed smoothed gradient of Eqs.

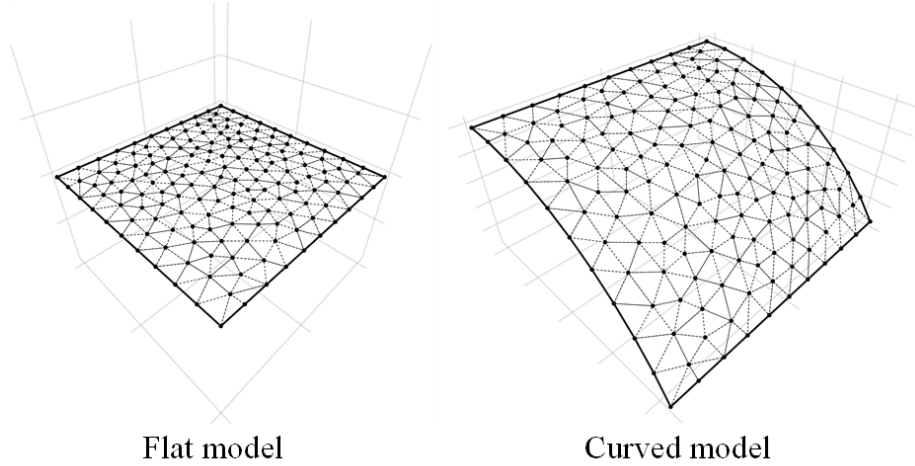


Figure 3: Meshfree discretization for patch test

(35) and (36) could not exactly reproduce the non-polynomial membrane and bending stress. However, the RKGSI-HW and RKGSI-Nitsche methods also provide better accuracy compared to others due to the fulfillment of first second-order variational consistency. And, even only with local variational consistency, the RKGSI-Penalty obtained a better result than traditional Gauss scheme. Meanwhile, the bending moment contours of M^{12} are listed in Fig. 4, which further verify that the proposed method provided a satisfactory result compared to exact solution. On the other hand, the RKGSI-Penalty and the conventional Gauss meshree formulations showed errors.

Table 1: Results of patch test for flat model.

	Linear patch test		Quadratic patch test	
	L_2 -Error	H_e -Error	L_2 -Error	H_e -Error
GI-Penalty	$4.45E-4$	$1.35E-2$	$2.01E-3$	$1.63E-2$
GI-Nitsche	$4.51E-4$	$1.42E-2$	$1.22E-3$	$1.68E-2$
RKGSI-Penalty	$3.64E-9$	$6.77E-8$	$4.54E-9$	$6.57E-8$
RKGSI-Nitsche	$3.31E-12$	$1.34E-11$	$5.98E-12$	$1.21E-11$
RKGSI-HR	$6.67E-13$	$1.50E-11$	$1.07E-12$	$1.26E-11$

5.2. Scordelis-Lo roof

This example considers the classical Scordelis-Lo roof problem, as depicted in Fig. 5. The cylindrical roof has dimensions $R = 25$, $L = 50$, $h = 0.25$, Young's modulus $E = 4.32 \times 10^8$ and Poisson's ratio $\nu = 0.0$. The entire roof is subjected to a uniform body force of $b_z = -90$, with the straight edges remaining free and the the curved edges are enforced by $v_x = v_z = 0$.

Table 2: Results of patch test for cylindrical model.

	Linear patch test		Quadratic patch test	
	L_2 -Error	H_e -Error	L_2 -Error	H_e -Error
GI-Penalty	$3.79E-4$	$1.30E-2$	$1.74E-3$	$1.37E-2$
GI-Nitsche	$4.04E-4$	$1.42E-2$	$1.15E-3$	$1.49E-2$
RKGSi-Penalty	$1.47E-4$	$5.39E-3$	$2.26E-4$	$2.09E-3$
RKGSi-Nitsche	$2.41E-6$	$7.37E-5$	$2.47E-6$	$2.89E-5$
RKGSi-HR	$4.28E-6$	$1.30E-4$	$9.69E-6$	$2.41E-4$

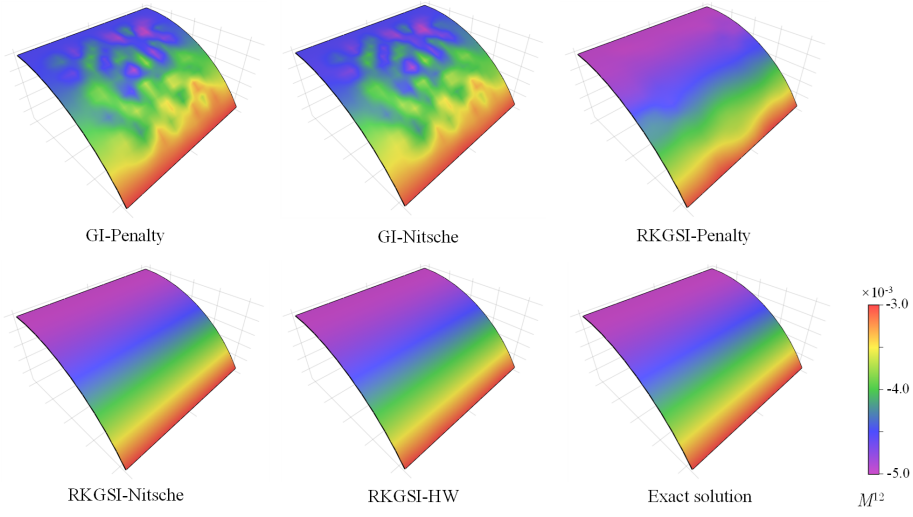


Figure 4: Contour plots of M^{12} for curved shell patch test.

369 Due to the symmetry, only a quadrant of the model is considered for meshfree
 370 analysis, which is discretized by the 11×16 , 13×20 , 17×24 and 19×28 meshfree
 371 nodes, as listed in Fig. 6. The comparison of the displacement in z -direction
 372 at node A , v_{A3} , is used as the investigated quantity, with the reference value
 373 0.3024 given by [32]. Firstly, Fig. 7 presents a sensitivity study for the artificial
 374 parameters of α_v 's, α_θ 's in the RKGSi meshfree formulations with Nitsche's
 375 method and penalty method. The results of Fig. 7 revealed, Nitsche's method
 376 observed less artificial sensitivity. However, both the methods cannot trivially
 377 determine the optimal values of the artificial parameters. The optimal artificial
 378 parameters from Fig. 7 are adopted for the convergence study in Fig. 8. The
 379 convergence result showed that the RKGSi get satisfactory results while the
 380 traditional Gauss methods demonstrated noticeable errors.

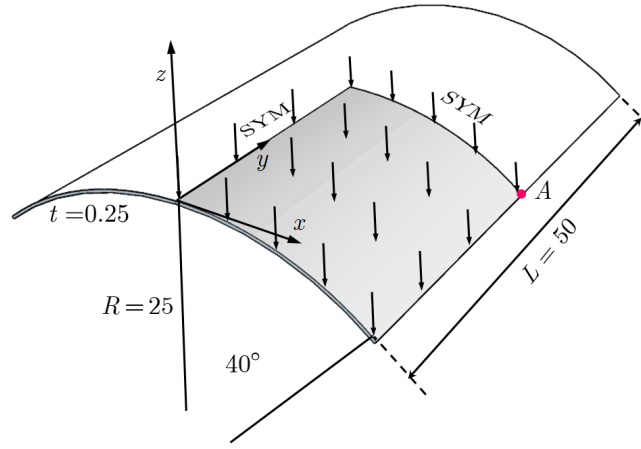


Figure 5: Description of Scordelis-Lo roof problem.

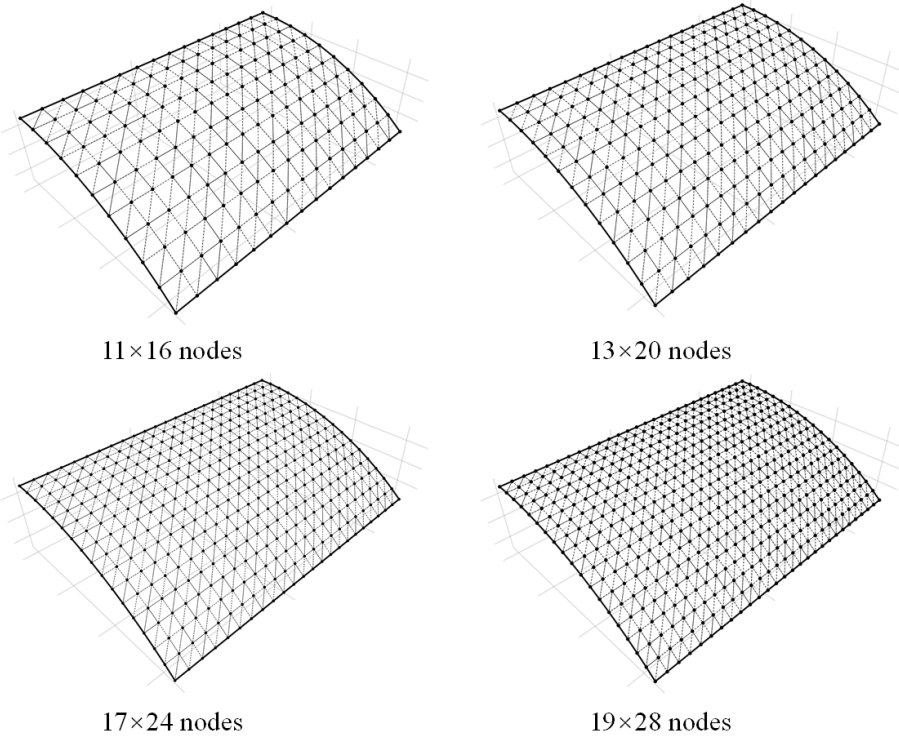


Figure 6: Meshfree discretizations for Scordelis-Lo roof problem.

5.3. Pinched Hemispherical shell

Consider the hemispherical shell shown in Fig. 9, which is loaded at four points $P = \pm 2$ at 90° interval at its bottom. The hemispherical shell has an radius $R = 10$, thickness $h = 0.04$, Young's modulus $E = 6.825 \times 10^7$ and Poisson's ratio $\nu = 0.3$.

Due to symmetry, only quadrant model, where the 8×8 , 16×16 , 24×24 and 32×32 meshfree nodes have been discretized, was considered. The quantity under investigation for convergence is the displacement at x -direction on point A , v_{A1} . Fig. 10 displays the corresponding convergence results, indicating the RKGSI scheme performed significantly better compared to the GI meshfree formulation. Meanwhile, the efficiency comparison for this problem is also shown in Fig. 11, in which the CPU time for assembly and calculation of shape functions are considered. Fig. 11(a) indicates that the RKGSI scheme observed high efficiency in assembly. This is due to the variational inconsistent Gauss meshfree formulation which require more Gaussian points to get satisfactory results. Fig. 11(b) lists the CPU time spent on enforcing essential boundary conditions for the penalty method, Nitsche's method and proposed HW method. The results highlighted that the proposed HW method consumed comparable CPU time in assembly compared to Nitsche's method. However, less time was spent to calculate the shape functions. Since both the HW method and penalty method were developed considering the shape functions first order derivatives. For this reason, both the methods shared an almost identical time in computing the shape functions.

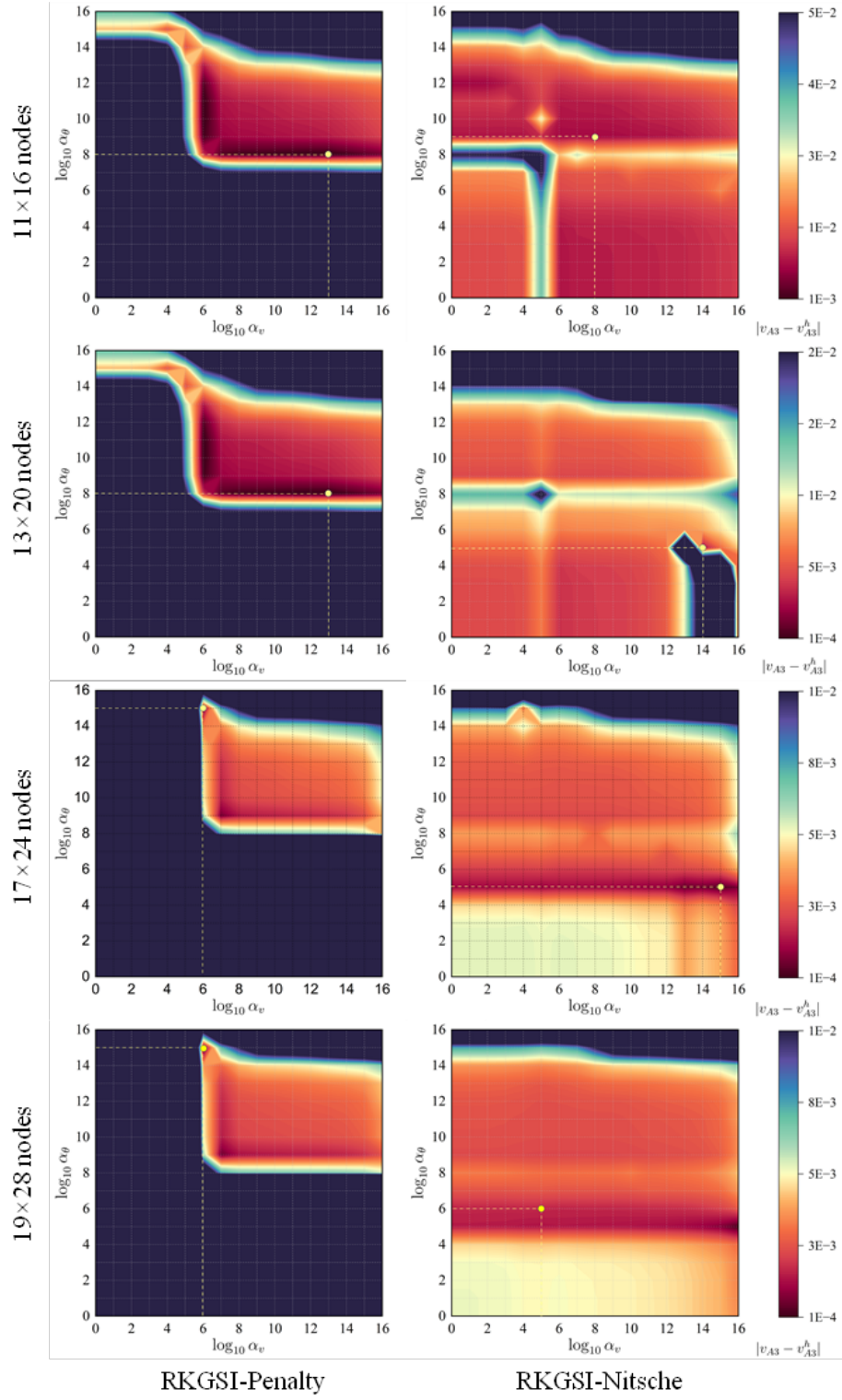


Figure 7: Sensitivity comparison of α_v and α_θ for Scordelis-Lo problem.

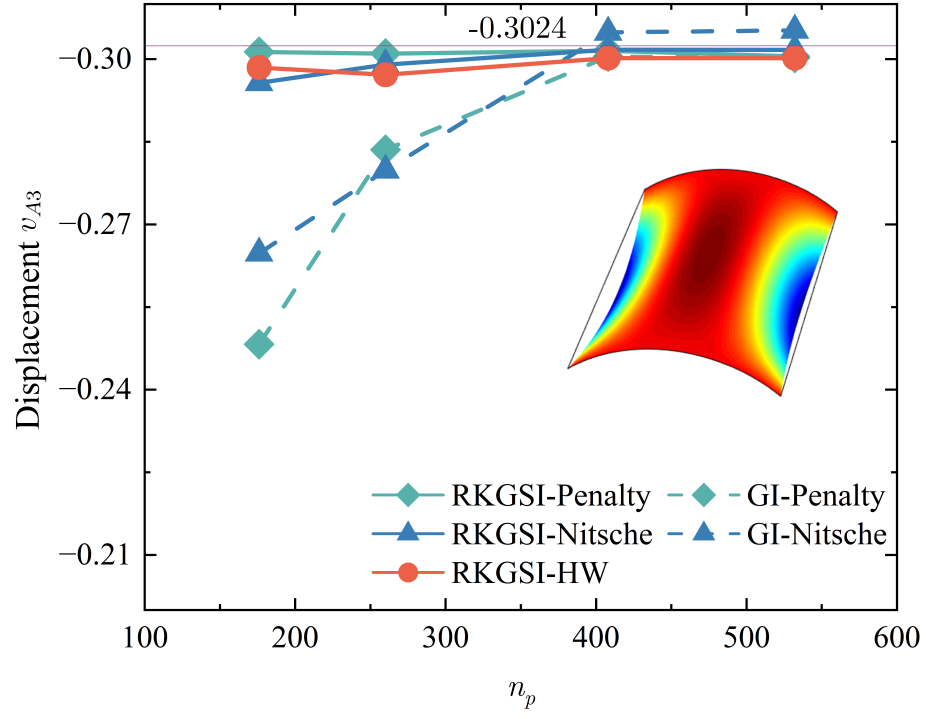


Figure 8: Displacement convergence for Scordelis-Lo roof problem.

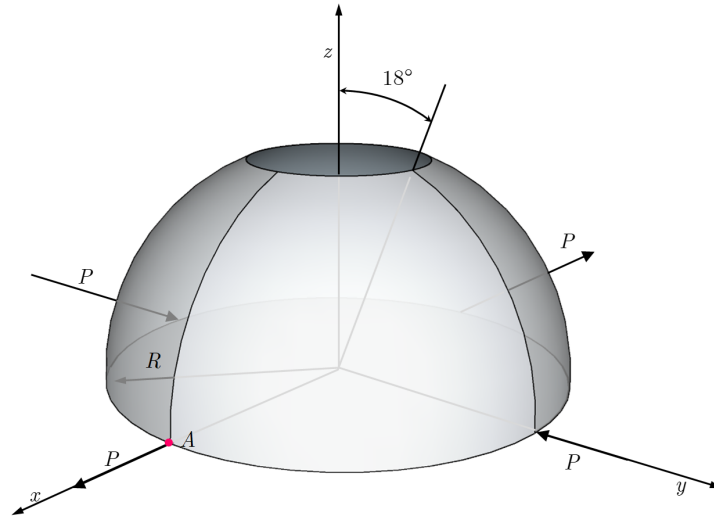


Figure 9: Description of pinched hemispherical shell problem.

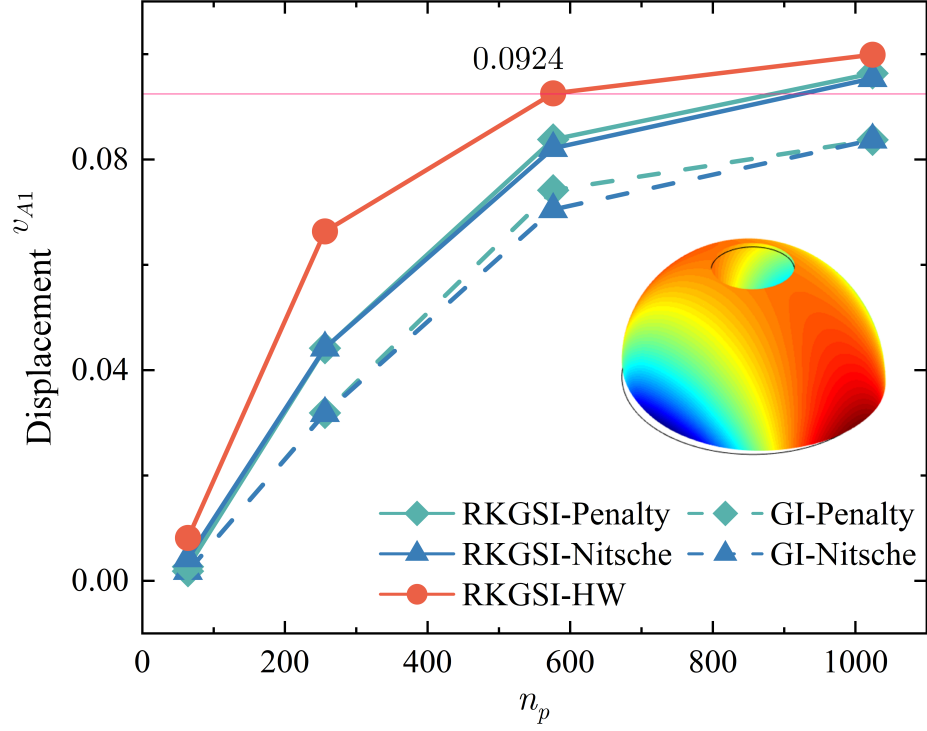


Figure 10: Displacement convergence for pinched hemispherical shell problem.

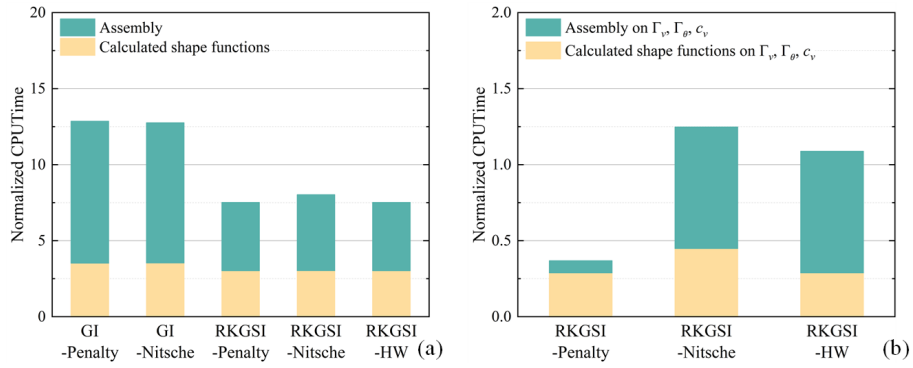


Figure 11: efficiency comparison for pinched hemispherical shell problem: (a) Whole domain; (b) Essential boundaries

404 6. Conclusion

405 In this study, an efficient and quasi-consistent meshfree thin shell formu-
406 lation was presented to naturally enforce the essential boundary conditions.
407 Mixed formulation with the Hu-Washizu principle weak form is adopted, where
408 the traditional meshfree shape functions discretized the displacement, and the
409 strains and stresses were expressed by the reproducing kernel smoothed gradi-
410 ents and the covariant smoothed gradients, respectively. The smoothed gradi-
411 ent naturally embedded the first second-order integration constraints and has
412 a quasi variational consistency for the curved models in each integration cell.
413 Owing to the Hu-Washizu variational principle, the essential boundary condi-
414 tion enforcement has a similar form with the conventional Nitsche's method;
415 both have consistent and stabilized terms. The costly high order derivatives
416 in the Nitsche's consistent term have been replaced by the smoothed gradients,
417 which improved the computational speed due to the reproducing kernel gradient
418 smoothing framework. Furthermore, the stabilized term naturally existed in the
419 Hu-Washizu weak form, and the artificial parameter needed in Nitsche's stabi-
420 lized term has vanished, which can automatically maintain the coercivity for
421 the stiffness matrix. Based on general reproducing kernel gradient smoothing
422 framework, the proposed methodology can be trivially extended to high order
423 basis meshfree formulation. The numerical results demonstrated that the pro-
424 posed Hu-Washizu quasi-consistent meshfree thin shell formulation showed ex-
425 cellent accuracy, efficiency, and stability.

Acknowledgment

The support of this work by the National Natural Science Foundation of China (12102138, 52350410467) and the Natural Science Foundation of Fujian Province of China (2023J01108, 2022J05056) is gratefully acknowledged.

430 Appendix A. Green's theorems for in-plane vector

431 This Appendix discusses two kinds of Green's theorems used for the devel-
 432 opment of the proposed meshfree method. For an arbitrary vectors v^α and a
 433 scalar function f , with Green's theorem for in-plane vector, the first Green's
 434 theorem is listed as follows [29]:

$$\begin{aligned} \int_{\Omega} f_{,\alpha} v^\alpha d\Omega &= \int_{\Gamma} f v^\alpha n_\alpha d\Gamma - \int_{\Omega} f (v_{,\alpha}^\alpha + \Gamma_{\beta\alpha}^\beta v^\alpha) d\Omega \\ &= \int_{\Gamma} f v^\alpha n_\alpha d\Gamma - \int_{\Omega} f v^\alpha|_\alpha d\Omega \end{aligned} \quad (\text{A.1})$$

435 where $\Gamma_{\alpha\beta}^\gamma = \mathbf{a}_{\alpha,\beta} \cdot \mathbf{a}^\gamma$ denotes the Christoffel symbol of the second kind. $v^\alpha|_\alpha$
 436 can be represented as the in-plane covariant derivative of the vector v^α :

$$v^\alpha|_\alpha = v_{,\alpha}^\alpha + \Gamma_{\beta\alpha}^\beta v^\alpha \quad (\text{A.2})$$

437 The second Green's theorem is established with a mixed form of second
 438 order derivative. Let $A^{\alpha\beta}$ can be an arbitrary symmetric second order tensor,
 439 the Green's theorem yields [29]:

$$\begin{aligned} \int_{\Omega} f_{,\alpha}|_\beta A^{\alpha\beta} d\Omega &= \int_{\Gamma} f_{,\gamma} n^\gamma A^{\alpha\beta} n_\alpha n_\beta d\Gamma - \int_{\Gamma} f (A^{\alpha\beta} s_\alpha n_\beta)_{,\gamma} s^\gamma d\Gamma + [[f A^{\alpha\beta} s_\alpha n_\beta]]_{\mathbf{x} \in C} \\ &\quad - \int_{\Gamma} f (A_{,\beta}^{\alpha\beta} n_\alpha + \Gamma_{\alpha\beta}^\gamma A^{\alpha\beta} n_\gamma + \Gamma_{\gamma\beta}^\gamma A^{\alpha\beta} n_\alpha) d\Gamma \\ &\quad + \int_{\Omega} f \left(\Gamma_{\alpha\beta,\gamma}^\gamma A^{\alpha\beta} + \Gamma_{\alpha\beta}^\gamma A_{,\gamma}^{\alpha\beta} + \Gamma_{\eta\gamma}^\eta \Gamma_{\alpha\beta}^\gamma A^{\alpha\beta} \right. \\ &\quad \left. + A_{,\alpha\beta}^{\alpha\beta} + \Gamma_{\gamma\beta,\alpha}^\gamma A^{\alpha\beta} + 2\Gamma_{\gamma\alpha}^\gamma A_{,\beta}^{\alpha\beta} + \Gamma_{\gamma\alpha}^\gamma \Gamma_{\eta\beta}^\eta A^{\alpha\beta} \right) d\Omega \\ &= \int_{\Gamma} f_{,\gamma} n^\gamma A^{\alpha\beta} n_\alpha n_\beta d\Gamma - \int_{\Gamma} f (A^{\alpha\beta} s_\alpha n_\beta)_{,\gamma} s^\gamma d\Gamma + [[f A^{\alpha\beta} s_\alpha n_\beta]]_{\mathbf{x} \in C} \\ &\quad - \int_{\Gamma} f A^{\alpha\beta}|_\beta n_\alpha d\Gamma + \int_{\Omega} f A^{\alpha\beta}|_{\alpha\beta} d\Omega \end{aligned} \quad (\text{A.3})$$

440 with

$$A^{\alpha\beta}|_\beta = A_{,\beta}^{\alpha\beta} + \Gamma_{\beta\gamma}^\alpha A^{\beta\gamma} + \Gamma_{\gamma\beta}^\gamma A^{\alpha\beta} \quad (\text{A.4})$$

441

$$\begin{aligned} A^{\alpha\beta}|_{\alpha\beta} &= \Gamma_{\alpha\beta,\gamma}^\gamma A^{\alpha\beta} + \Gamma_{\alpha\beta}^\gamma A_{,\gamma}^{\alpha\beta} + \Gamma_{\eta\gamma}^\eta \Gamma_{\alpha\beta}^\gamma A^{\alpha\beta} \\ &\quad + A_{,\alpha\beta}^{\alpha\beta} + \Gamma_{\gamma\beta,\alpha}^\gamma A^{\alpha\beta} + 2\Gamma_{\gamma\alpha}^\gamma A_{,\beta}^{\alpha\beta} + \Gamma_{\gamma\alpha}^\gamma \Gamma_{\eta\beta}^\eta A^{\alpha\beta} \end{aligned} \quad (\text{A.5})$$

442 For the sake of brevity, the notion of covariant derivative is extended to a
 443 scalar function as:

$$f|_\alpha = f_{,\alpha} + \Gamma_{\beta\alpha}^\beta f \quad (\text{A.6})$$

444

$$f|_\beta n_\alpha = f_{,\beta} n_\alpha + \Gamma_{\alpha\beta}^\gamma f n_\gamma + \Gamma_{\gamma\beta}^\gamma f n_\alpha \quad (\text{A.7})$$

445

$$\begin{aligned} f|_{\alpha\beta} &= \Gamma_{\alpha\beta,\gamma}^\gamma f + \Gamma_{\alpha\beta}^\gamma f_{,\gamma} + \Gamma_{\eta\gamma}^\eta \Gamma_{\alpha\beta}^\gamma f \\ &\quad + f_{,\alpha\beta} + \Gamma_{\gamma\beta,\alpha}^\gamma f + 2\Gamma_{\gamma\alpha}^\gamma f_{,\beta} + \Gamma_{\gamma\alpha}^\gamma \Gamma_{\eta\beta}^\eta f \end{aligned} \quad (\text{A.8})$$

446 **Appendix B. Derivations for stiffness metrics and force vectors**

447 This Appendix details the derivations of stiffness matrices and force vectors
 448 in Eqs. (53)-(55), where the relationships of Eqs. (40), (41), (44) and (46) are
 449 used herein. Firstly, the membrane strain terms are considered as follows:

$$\begin{aligned}
 & \sum_{C=1}^{n_e} \int_{\Omega_C} \delta \tilde{\varepsilon}_{\alpha\beta}^h h C^{\alpha\beta\gamma\eta} \tilde{\varepsilon}_{\gamma\eta}^h d\Omega \\
 &= \sum_{C=1}^{n_e} \sum_{I,J=1}^{n_p} \delta \mathbf{d}_I \cdot \underbrace{\int_{\Omega_C} \tilde{\varepsilon}_{\alpha\beta I} h C^{\alpha\beta\gamma\eta} \mathbf{a}_\gamma \mathbf{q}^T d\Omega \mathbf{G}^{-1} \bar{\mathbf{g}}_{\eta J}}_{\tilde{\mathbf{g}}_I^{\eta T}} \cdot \mathbf{d}_J \\
 &= \sum_{C=1}^{n_e} \sum_{I,J=1}^{n_p} \delta \mathbf{d}_I \cdot \int_{\Gamma_C \cap \Gamma_v} \Psi_J \mathbf{q}^T \underbrace{\mathbf{G}^{-1} \tilde{\mathbf{g}}_I^\alpha n_\alpha}_{\tilde{\mathbf{T}}_{NI}} d\Gamma \cdot \mathbf{d}_J \\
 &= \sum_{I,J=1}^{n_p} \delta \mathbf{d}_I \cdot \int_{\Gamma_v} \tilde{\mathbf{T}}_{NI} \Psi_J d\Gamma \cdot \mathbf{d}_J
 \end{aligned} \tag{B.1}$$

450 with

$$451 \quad \tilde{\mathbf{g}}_I^\alpha = \mathbf{q} \mathbf{a}_\beta h C^{\alpha\beta\gamma\eta} \tilde{\varepsilon}_{\alpha\beta I} \tag{B.2}$$

$$452 \quad \tilde{\mathbf{T}}_{NI} = \mathbf{q}^T \mathbf{G}^{-1} \tilde{\mathbf{g}}_I^\alpha n_\alpha \tag{B.3}$$

Following this path, the bending strain terms can be reorganized by:

$$\begin{aligned}
 & \sum_{C=1}^{n_e} \int_{\Omega_C} \delta \tilde{\kappa}_{\alpha\beta}^h \frac{h^3}{12} C^{\alpha\beta\gamma\eta} \tilde{\kappa}_{\gamma\eta}^h d\Omega \\
 &= \sum_{C=1}^{n_e} \sum_{I,J=1}^{n_p} \delta \mathbf{d}_I \cdot \underbrace{\int_{\Omega_C} \tilde{\kappa}_{\alpha\beta I} \frac{h^3}{12} C^{\alpha\beta\gamma\eta} \mathbf{a}_3 \mathbf{q}^T d\Omega \mathbf{G}^{-1} \bar{\mathbf{g}}_{\gamma\eta J}}_{\tilde{\mathbf{g}}_I^{\gamma\eta T}} \cdot \mathbf{d}_J \\
 &= \sum_{C=1}^{n_e} \sum_{I,J=1}^{n_p} \delta \mathbf{d}_I \cdot \left(\begin{aligned} & \int_{\Gamma_C \cap \Gamma_\theta} \underbrace{\mathbf{q}^T \mathbf{G}^{-1} \tilde{\mathbf{g}}_I^{\alpha\beta} n_\alpha n_\beta}_{\tilde{\mathbf{M}}_{nnI}} n^\gamma \Psi_{J,\gamma} d\Gamma \\ & - \int_{\Gamma_C \cap \Gamma_v} \underbrace{(\mathbf{q}_{|\beta}^T \mathbf{G}^{-1} \tilde{\mathbf{g}}_I^{\alpha\beta} n_\alpha + (\mathbf{q}^T \mathbf{G}^{-1} \tilde{\mathbf{g}}_I^{\alpha\beta} s_\alpha n_\beta)_{,\gamma} s^\gamma)}_{\tilde{\mathbf{T}}_{MI}} \Psi_J d\Gamma \\ & + [[\underbrace{\mathbf{q}^T \mathbf{G}^{-1} \tilde{\mathbf{g}}_I^{\alpha\beta} s_\alpha n_\beta}_{\tilde{\mathbf{P}}_I \mathbf{a}_3} \Psi_J]]_{\mathbf{x} \in C_C \cap C_v} \end{aligned} \right) \cdot \mathbf{d}_J \\
 &= \sum_{I,J=1}^{n_p} \delta \mathbf{d}_I \cdot \left(\int_{\Gamma_\theta} \tilde{\mathbf{M}}_{nnI} n^\gamma \Psi_{J,\gamma} d\Gamma - \int_{\Gamma_v} \tilde{\mathbf{T}}_{MI} \Psi_J d\Gamma + [[\tilde{\mathbf{P}}_I \Psi_J]]_{\mathbf{x} \in C_v} \right)
 \end{aligned} \tag{B.4}$$

453 with

$$\tilde{\mathbf{g}}_I^{\alpha\beta} = \int_{\Omega_C} \mathbf{q} \frac{h^3}{12} C^{\alpha\beta\gamma\eta} \mathbf{a}_3 \tilde{\kappa}_{\alpha\beta I} d\Omega \quad (\text{B.5})$$

454

$$\begin{cases} \tilde{M}_{nnI} = \mathbf{q}^T \mathbf{G}^{-1} \tilde{\mathbf{g}}_I^{\alpha\beta} n_\alpha n_\beta \\ \tilde{\mathbf{T}}_{MI} = \mathbf{q}_{|\beta}^T \mathbf{G}^{-1} \tilde{\mathbf{g}}_I^{\alpha\beta} n_\alpha + (\mathbf{q}^T \mathbf{G}^{-1} \tilde{\mathbf{g}}_I^{\alpha\beta} s_\alpha n_\beta)_{,\gamma} s^\gamma \\ \tilde{\mathbf{P}}_I = \mathbf{q}^T \mathbf{G}^{-1} \tilde{\mathbf{g}}_I^{\alpha\beta} s_\alpha n_\beta \cdot \mathbf{a}_3 \end{cases} \quad (\text{B.6})$$

References

- [1] L. H. Donnell, Beams, Plates and Shells, McGraw-Hill. `arXiv:0_IeAQAAIAAJ`.
- [2] T. J. Hughes, The Finite Element Method: Linear Static and Dynamic Finite Element Analysis, Dover Publications.
- [3] T. Belytschko, Y. Y. Lu, L. Gu, Element-free Galerkin methods 37 (2) 229–256. `arXiv:10208278`.
- [4] W. K. Liu, S. Jun, Y. F. Zhang, Reproducing kernel particle methods 20 (8-9) 1081–1106.
- [5] J. S. Chen, M. Hillman, S. W. Chi, Meshfree methods: Progress made after 20 years 143 (4) 04017001.
- [6] P. Krysl, T. Belytschko, Analysis of thin shells by the Element-Free Galerkin method 33 (20) 3057–3080.
- [7] G. R. Liu, Meshfree Methods: Moving Beyond the Finite Element Method, Second Edition, Crc Press.
- [8] X. Zhang, K. Z. Song, M. W. Lu, X. Liu, Meshless methods based on collocation with radial basis functions 26 333–343.
- [9] D. Millán, A. Rosolen, M. Arroyo, Thin shell analysis from scattered points with maximum-entropy approximants 85 (6) 723–751.
- [10] L. Wang, M. Hu, Z. Zhong, F. Yang, Stabilized Lagrange Interpolation Collocation Method: A meshfree method incorporating the advantages of finite element method 404 115780.
- [11] P. Suchde, T. Jacquemin, O. Davydov, Point Cloud Generation for Mesh-free Methods: An Overview 30 (2) 889–915.
- [12] L. Deng, D. Wang, An accuracy analysis framework for meshfree collocation methods with particular emphasis on boundary effects 404 115782.
- [13] S. Fernández-Méndez, A. Huerta, Imposing essential boundary conditions in mesh-free methods 193 (12-14) 1257–1275.
- [14] X. Li, Error estimates for the moving least-square approximation and the element-free Galerkin method in n-dimensional spaces 99 77–97.
- [15] J. Wu, D. Wang, An accuracy analysis of Galerkin meshfree methods accounting for numerical integration 375 113631.
- [16] J.-S. Chen, H.-P. Wang, New boundary condition treatments in meshfree computation of contact problems 187 (3) 441–468.

- 489 [17] D. Liu, Y. M. Cheng, The interpolating element-free Galerkin (IEFG)
490 method for three-dimensional potential problems 108 115–123.
- 491 [18] V. Ivannikov, C. Tiago, P. M. Pimenta, On the boundary conditions of the
492 geometrically nonlinear Kirchhoff–Love shell theory 51 (18) 3101–3112.
- 493 [19] Y. Y. Lu, T. Belytschko, L. Gu, A new implementation of the element free
494 Galerkin method 113 (3-4) 397–414. [arXiv:26071039](#).
- 495 [20] T. Zhu, S. N. Atluri, A modified collocation method and a penalty formu-
496 lation for enforcing the essential boundary conditions in the element free
497 Galerkin method 21 (3) 211–222.
- 498 [21] S. Skatulla, C. Sansour, Essential boundary conditions in meshfree methods
499 via a modified variational principle: Applications to shell computations
500 15 (2) 123–142.
- 501 [22] J. S. Chen, C. T. Wu, S. Yoon, Y. You, A stabilized conforming nodal
502 integration for Galerkin mesh-free methods 50 (2) 435–466.
- 503 [23] J. S. Chen, M. Hillman, M. Rüter, An arbitrary order variationally con-
504 sistent integration for Galerkin meshfree methods 95 (5) 387–418. [arXiv:](#)
505 [260949200001](#).
- 506 [24] Q. Duan, X. Li, H. Zhang, T. Belytschko, Second-order accurate derivatives
507 and integration schemes for meshfree methods 92 (4) 399–424. [arXiv:](#)
508 [260949200001](#).
- 509 [25] D. Wang, J. Wu, An inherently consistent reproducing kernel gradient
510 smoothing framework toward efficient Galerkin meshfree formulation with
511 explicit quadrature 349 628–672.
- 512 [26] J. Wang, X. Ren, A consistent projection integration for Galerkin meshfree
513 methods 414 116143.
- 514 [27] J. Wu, X. Wu, Y. Zhao, D. Wang, A consistent and efficient method for
515 imposing meshfree essential boundary conditions via hellinger-reissner vari-
516 ational principle. 54 (12) 3283–3296.
- 517 [28] J. Wu, X. Wu, Y. Zhao, D. Wang, A rotation-free Hellinger-Reissner mesh-
518 free thin plate formulation naturally accommodating essential boundary
519 conditions 154 122–140.
- 520 [29] J. Benzaken, J. A. Evans, S. F. McCormick, R. Tamstorf, Nitsche’s method
521 for linear Kirchhoff–Love shells: Formulation, error analysis, and verifica-
522 tion 374 113544.
- 523 [30] H. Dah-wei, A method for establishing generalized variational principle
524 6 (6) 501–509.

- 525 [31] H. Du, J. Wu, D. Wang, J. Chen, A unified reproducing kernel gradient
526 smoothing Galerkin meshfree approach to strain gradient elasticity 70 (1)
527 73–100.
- 528 [32] R. H. Macneal, R. L. Harder, A proposed standard set of problems to test
529 finite element accuracy 1 (1) 3–20.